Construction of a Polarizable Force Field for Molecular Dynamics Simulation of a NaOTF Water-In-Salt Electrolyte

Majid Rezaei[1,], Sung Sakong[1] and Axel Groß[1,2]*

[1]Institute of Theoretical Chemistry, Ulm University, Oberberghof 7, 89081 Ulm, Germany

[2]Helmholtz Institute Ulm (HIU) for Electrochemical Energy Storage, Helmholtzstraße 11, 89069 Ulm,

Germany

[*] Corresponding author - Email: majid.rezaei@uni-ulm.de

ABSTRACT

To model a NaOTF Water-in-Salt (WiS) electrolyte using classical Molecular Dynamics (MD) simulations, we explore various force fields where atomic polarization is accounted for at three different levels: a non-polarizable all-atom force field where polarization is only implicitly included in its Van der Waals interaction parameters, the same force field with uniformly scaled ionic charges mimicing electron polarization within a mean-field approximation, and an explicit polarizable force field where polarization is modeled via Drude oscillators. We also probe combining different polarization levels for salt ions and water: when ion polarization is described by the Drude method, water is modeled by either the non-polarizable SPC/E model or the polarizable SWM4-NDP model. The main goal is to achieve simulation stability for different force fields and investigate the influence of the force field parameters on the electrolyte properties. Force field parameters that adjust the interactions of cations or Drude pairs are found to significantly affect the electrolyte structure and its dynamic properties. This effect is primarily due to the strong dependence of the degree of salt dissociation on these parameters. Among the force fields studied in this work, we identify an efficient combination of the Drude polarizable force field with non-polarizable water models, which is sufficiently flexible to reproduce various properties of WiS solutions, while the computational cost is affordable and simulation stability is ensured over a relatively wide range of force field parameters.

NOMENCLATURE

Symbol/Notation	Description
U	Potential energy
ε	Lennard-Jones interaction strength
σ	Lennard-Jones minimum separation distance
r	The distance from an atom or between two atoms
q	Atomic (partial) charge
k_q	Ionic charge scaling factor
ε_0	Vacuum permittivity
w	Weighting coefficient for pairwise energy between atoms in the same molecule
k_b	Bond constant
k_θ	Angle constant
k_m	Dihedral force constants
r_0	Optimal bond length
θ_0	Valance angle
φ_0	Valance dihedral angle
V_D	Harmonic potential between a Drude particle and its respective core
k_D	Bond constant between a Drude particle and its respective core
r_D	The distance between a Drude particle and its respective core
q_D	Drude charge representing an induced dipole on a polarizable atom
m_D	Mass of the Drude particle
α	Atomic polarizability
q'	Non-polarizable part of the charge on a Drude core
k_{LJ}	Scaling factor for Lennard-Jones interactions between two polarizable fragments
$\bar{q}$	The net charge of a polarizable fragment
$\bar{\alpha}$	Molecular polarizability of a polarizable fragment
$\bar{\mu}$	Dipole moment of a polarizable fragment
$\bar{r_0}$	Equilibrium distance between the centers of mass of two polarizable fragments
$T(r)$	Thole damping function
a	Thole damping parameter
$f_{TT}(r)$	Tang-Toennies (TT) damping function
b_{TT} and c_{TT}	Tang-Toennies damping parameters
t	Time
dt	Time step
D	Diffusion coefficient
V	Volume of the simulation box
$P_{\alpha\beta}$	Stress in the $\alpha\beta$ plane
$g(r)$	Radial pair distribution function
$r_{1,2}$	Positions of the first and the second peaks in the radial pair distribution function
ρ	Density
k_α^{OTF}	The scaling factor applied to the polarizabilities of the atoms in OTF-
WiS	Water-in-Salt
DP	Drude particle
DC	Drude Core
CN	Coordination number
VACF	Velocity auto-correlation function
RDF	Radial distribution function
MSD	Mean squared displacement
AGG	Aggregate
CIP	Contact ion pair
SSIP	Solvent-separated ion pair
BNP	Base non-polarizable (force field)
BPP	Base partially polarizable (force field)
FP	Fully polarizable (force field)

1 Introduction

Electrochemical energy storage using secondary batteries is a critical component for our future sustainable energy economy. Currently, Li-ion batteries (LiBs) are dominating the market of high-performance batteries. Since their commercialization more than thirty years ago the performance of LiBs has been constantly improved [1]. However, in spite of technological progress that is still possible, the Li-ion battery technology is facing physico-chemical limits of its performance [2]. Furthermore, there are concerns with regard to safety aspects [3] and with the sustainability of the materials used in Li-ion batteries [4]. As one of the main causes for hazards in the battery operation, dendrite growth at the anodes has been identified [5], which can lead to short-circuits which together with flammable electrolytes might result in battery fires. One option to reduce these fire risks is to use non-flammable electrolytes such as ionic liquids [6-7]. However, the high costs of such ionic liquids still prevent their commercialisation. Aqueous electrolytes would be ideal [8-9] as they combine non-flammability with excellent transport properties. However, they are limited by their small potential window of electrochemical stability. As a promising alternative, water-in-salt (WiS) electrolytes have recently been introduced [10-11]. They are based on the concept of using dissolved salts in extremely high concentrations, higher than the concentration of water molecules. As a consequence, all water molecules are involved in building up the solvation shell of the charge carrier so that hardly any free water molecules are present. Thus, there are no longer any weak hydrogen bonds between water molecules present, but only stronger water-ion bonds. This can increase the electrochemical stability window to values above 3V [12]. This water-in-salt concept has first been applied to Li-ion batteries, but it has also been extended to sodium-ion batteries [NaBs] [13]. Sodium is much more earth-abundant than Lithium. Recently, sodium-ion batteries have drawn a lot of attention as an alternative cell chemistry for mobile and also in particular stationary applications [14-15]. Typically, their production does not require any critical raw materials. Their energy densities and cyclability can still not fully compete with Li-ion batteries, but they promise to be less expensive together with better charging and ion mobility properties.

Still, there is a need to better understand the properties of Sodium-ion batteries with WiS electrolytes. From a theoretical point of view, this requires performing molecular dynamics (MD) simulations in order to take the liquid nature of the WiS electrolytes appropriately into account. Ab initio molecular dynamics (AIMD) simulations [16] would be the ideal choice as they combine a proper description of the chemical interactions with statistical sampling. However, due to their high computational effort, typically only small system sizes and short simulation times can be considered. In contrast, classical force fields allow to run MD simulations for sufficiently large system sizes and long simulation times, but they suffer from a limited accuracy as far as the chemical interactions are concerned. So far, good efforts have been made to model WiS electrolytes using classical MD simulations [17-22]. However, most of the previous studies have focused on such electrolytes in Li-ion batteries and there are far fewer studies on Na-ion batteries. Furthermore, there are still serious doubts about the accuracy of the force fields used for the simulation of WiS solutions, particularly with regard to how they account for polarization effects, which are of paramount importance at high salt concentrations. The non-polarizable force fields OPLS [23] and GAFF [24] were used separately to model the interactions of Na^+ ions in different WiS solutions [25-27]. Kartha and Mallik [28], however, reported that the use of non-polarizable force fields alone is insufficient to accurately reproduce the transport properties of such solutions. They used an ionic charge scaling approach in their MD simulations of NaTFSI and LiTFSI WiS electrolytes to model the dynamics of the system. To provide a sufficiently accurate model to predict both dynamics and structure of WiS electrolytes in Na-ion batteries, Jiang et. al [29] used the quantum-chemistry-based polarizable force field APPLE&P [30]. This model is a proprietary model whose parameters are not available in the open literature, while its uncommon functional form makes it difficult to extend and combine it to simulate different compounds or materials [31]. Therefore, using more common polarizable force fields, such as Drude-based models [32], seems like a more reasonable option. To the best of our knowledge, no extensive work has been done on the molecular simulation of WiS electrolytes using this type of force field. Furthermore, it is reported that the existing parametrizations of the Drude polarizable force fields do not accurately predict the

properties of ionic liquids in Na-ion batteries [33], indicating the need for further development of such force fields.

In the present work, as a first step to reliably study the properties of WiS electrolytes in Na-ion batteries, we have tested and compared four different force fields. We have particularly focused on their description of atomic polarization, as this is crucial for a reliable modeling of WiS electrolytes, as discussed above. By comparing the performance of the four different force fields, we will at the same time identify chemical and physical properties of the electrolytes that are crucial for their use in Na-ion batteries. The dependence of electrolyte properties on force field parameters has also been examined to make a general framework for the force field parameterization process.

2 Numerical Methods

2.1 Force field construction

We aim to model a NaOTF Water-in-Salt (WiS) electrolyte using classical molecular dynamics simulations. For this purpose, a well-suited force field potential is essential to evaluate the electrolyte properties correctly. The force field potential must be capable of describing the complex inter- and intramolecular interactions of water, anion (OTF$^-$), and cation (Na$^+$) particles. In classical MD, the potential energy of a system is modeled through bonded and non-bonded terms that, respectively, describe the interactions between the atoms that are linked by covalent bonds and the non-covalent interactions between all pairs of atoms

$$U_{tot} = U_{bonded} + U_{non-bonded} \tag{1}$$

Depending on the characteristics of the system and the details to be modeled by the force field, U_{bonded} and $U_{non-bonded}$ may consist of different terms. In particular, for systems containing strongly polarizable atoms, such as the studied WiS electrolyte, the potential energy terms must reflect the effect of polarization. In the present study, we construct force field potentials where polarization effect is either

implicitly or explicitly accounted for to capture the nature of the WiS electrolyte. The functional forms of these force fields are detailed in the following sections.

2.1.1 Non-polarizable force field

We start with an all-atom force field where the polarization effect is only implicitly included in the Van der Waals (VdW) and electrostatic interaction parameters. For this purpose, pairwise Lennard-Jones (LJ) and Coulomb potentials are used to approximate VdW and electrostatic interactions, respectively. The LJ term represents a combination of the short-distance interatomic repulsion and both the dispersion and induction (polarization) contributions to the Van der Waals interaction. The coulomb term describes the long-range electrostatic interaction. By scaling the ionic charges, the electronic polarization can also be included in the Coulomb term in a mean field approximation[34-36]. The non-bonded term of the potential energy is given by

$$U_{non-bonded} = w^{ij} \sum_i \sum_{j>i} \left(4\varepsilon^{ij} \left[\left(\frac{\sigma^{ij}}{r^{ij}} \right)^{12} - \left(\frac{\sigma^{ij}}{r^{ij}} \right)^6 \right] + \frac{k_q^i q^i k_q^j q^j}{4\pi\varepsilon_0 r^{ij}} \right) \tag{2}$$

where i and j run over all the atoms in the system, r^{ij} is the distance between the atoms i and j, σ^{ij} and ε^{ij} are the Lennard-Jones size and interaction strength, respectively, ε_0 is the vacuum permittivity, $q^{i,j}$ is the atomic (partial) charge, $k_q^{i,j}$ is a factor that uniformly scales down ionic charges to approximate electronic polarization (see Eq. 3), and w^{ij} is a weighting coefficient for pairwise energy between atoms in the same molecule (given by Eq. 4).

$$k_q^i = \begin{cases} K_q \leq 1 & if\ i \in ions \\ 1 & otherwise \end{cases} \tag{3}$$

$$w_{ij} = \begin{cases} 0 & if\ ij \in b_1 \\ 0 & if\ ij \in b_2 \\ 0.5 & if\ ij \in b_3 \\ 1 & otherwise \end{cases} \tag{4}$$

b_1, b_2, and b_3 in Eq. 4 are the sets of atom pairs: connected by direct bond, via one intermediate bond, and via two intermediate bonds, respectively. The LJ parameters σ^{ij} and ε^{ij} in Eq. 2 are calculated using geometric means, $\sigma^{ij} = \sqrt{\sigma^i \sigma^j}$ and $\varepsilon^{ij} = \sqrt{\varepsilon^i \varepsilon^j}$, with $\sigma^{i,j}$ and $\varepsilon^{i,j}$ being the LJ parameters for atoms i and j, which depend only on the type of the corresponding atoms. In practice, we use a cutoff radius of 1.2 nm for the LJ interactions.

Whereas the interactions of the solvated cations (Na^+) can be fully represented by the non-bonded terms described in Eq. 2, water and anion (OTF^-) molecules require additional terms to describe their molecular configurations and intramolecular covalent interactions. Considering the two-body, three-body angular, and four-body dihedral interactions between the atoms in molecules, the covalent bonded potential energy can be written as

$$U_{bonded} = \sum_{ij \in bonds} k_b^{ij}\left(r^{ij} - r_0^{ij}\right)^2 + \sum_{ijk \in angles} k_\theta^{ijk}\left(\theta^{ijk} - \theta_0^{ijk}\right)^2$$
$$+ \sum_{\substack{ijks \in \\ dihedrals}} \sum_{m=1}^{4} \frac{k_m^{ijks}}{2}\left[1 + (-1)^{m+1}cos\left(m\varphi_0^{ijks}\right)\right] \tag{5}$$

where *bonds*, *angles*, and *dihedrals* indicate the atom groups for which the corresponding non-bonded interactions are defined, k_b^{ij}, k_θ^{ijk}, and k_m^{ijks} are the bond, angle, and dihedral force constants, respectively, r_0^{ij} is the optimal bond length, θ_0^{ijk} is the valance angle, and φ_0^{ijks} is the valance dihedral angle.

Although the non-polarizable force field requires no additional computational costs for describing polarization effects, it cannot adequately model strongly polarized systems like WiS, which will require an explicit description of atomic polarization, such as the Drude oscillator model.

2.1.2 Polarizable force field

A. Drude oscillator model

The Drude oscillator model [32, 37] (also referred to as the core-shell model or charge-on-spring model [38-39]) is used to explicitly account for the dynamics of the electric dipole moments on polarizable atoms. In this model, a so-called Drude particle (also called a shell [40]) is added to each polarizable atom to form a pair of oppositely charged particles: a positively charged Drude core (DC) carrying the majority of the atomic mass and a negatively charged Drude particle (DP) modeling a fluctuating electron cloud whose center can be displaced from the atom core. These two particles are bound by a harmonic potential

$$U_D = \frac{k_D}{2} r_D^2$$

(6)

with k_D being the spring constant and r_D being the distance between the DP and its respective DC. Drude particles also contribute to the electrostatic interactions in Eq. 2. Then, the pairwise Coulomb term includes both DC $(q' + q_D)$ and DP $(-q_D)$ charges of a polarizable atom as shown in Eq. 13, where q' is the atomic partial charge in the corresponding non-polarizable force field (see Eq. 2) and q_D is the point charge representing the induced dipole on the polarizable atom. q_D and k_D are related through

$$\alpha = \frac{q_D{}^2}{k_D}$$

(7)

with α being the atomic polarizability. It should be noted that atomic polarizability is the sum of two contributions: the distortion of the electron cloud around the nucleus and the interatomic charge redistribution caused by the local electric field. Drude oscillators only model the first contribution of the polarizability. The second contribution can be taken into account using variable partial charges, which is beyond the subject of this paper. To avoid overestimation of atomic polarizabilities in Drude polarizable simulations, overall polarizabilities can be reduced by appropriate control factors [37]. Alternatively, appropriate damping functions can be applied to reduce short-range dipolar interactions, as will be

discussed later in Sec. 2.1.2, B. In the present study, k_D is set to the same value for all polarizable atoms (see Sec.2.2.4) and q_D is calculated for individual atom types from Eq. 7. We employ a scalar spring constant for all Drude oscillators, which makes their response to local electric fields independent of field direction. Nevertheless, the intramolecular electrostatic interactions between induced oscillators lead to an anisotropic molecular polarizability, as it occurs in polar molecules. To describe the local anisotropy around lone pairs more precisely, one must expand the force constant between Drude pairs into a tensor form by setting off-diagonal elements to zero, which determines the orientation-dependent deformation of Drude oscillators (see Refs. [37, 41-42]).

Unlike DPs, which interact purely electrostatically and have no LJ interaction, non-bonded interactions of other particles include both LJ and coulomb contributions (see Eq. 2). During parameterization, therefore, the LJ parameters for DCs and non-polarizable atoms must be determined. For this purpose, one can use the same LJ parameters as in non-polarizable force fields. However, since the LJ potential in non-polarizable force fields implicitly includes the polarization contributions to the VdW interactions, the LJ interactions of DCs must be rescaled to avoid double counting of the polarization effect. In practice, we use the fragment-base scaling factor, as proposed by Golovizinia et al. [31, 43]

$$k_{LJ}^{ij} = \left(1 + 0.25 \overline{r_0}^{ij\,2} \frac{\overline{q}^{i\,2} \overline{\alpha}^j + \overline{q}^{j\,2} \overline{\alpha}^i}{\overline{\alpha}^i \overline{\alpha}^j} + 0.11 \frac{\overline{\mu}^{i\,2} \overline{\alpha}^j + \overline{\mu}^{j\,2} \overline{\alpha}^i}{\overline{\alpha}^i \overline{\alpha}^j} \right)^{-1} \tag{8}$$

where i and j denote a pair of DCs belonging to two different polarizable fragments, $\overline{q}^i$, $\overline{\alpha}^i$, and $\overline{\mu}^i$ are, respectively, the net charge, molecular polarizability, and dipole moment of the fragment containing atom i, and $\overline{r_0}^{ij}$ is the equilibrium distance between the centers of mass of the fragments containing atoms i and j. For salt fragments, we use $\overline{r_0}^{ij} = 4.17\text{Å}$ for the interactions between Na^+ and OTF^-, which is obtained from ab initio molecular dynamics calculations done in similar fashion as described in Refs. [16, 44]. As will be shown later in Eq. 13, the scaling factor is applied to the LJ term of the non-bonded potential energy for DC-DC interactions.

Eq. 8 can only be used with Drude particles on top of a purely non-polarizable force field. When the original force field already contains fragments whose polarizabilities are explicitly modeled, the scaling factor should be applied selectively. For example, the SWM4-NDP water model (see Sec. 2.2.1) explicitly accounts for the dynamic polarization contributions, and its LJ parameters are adjusted accordingly. Therefore, to model the explicitly polarized salt ions in the SWM4-NDP water model, the scaling factor should be fully applied only to ion-ion LJ interactions. For water-ion interactions, the scaling factor must only account for the influence of water molecules on ions, not for the reciprocal effects [31]. Therefore, Eq. 8 can be detailed for each pair interaction as

$$
k_{LJ}^{ij} = \begin{cases} 1 & \text{if } i \text{ and } j \in DC_w \\ \left(1 + 0.25\bar{r}^{ij2}\dfrac{\bar{q}^{i2}\bar{\alpha}^j + \bar{q}^{j2}\bar{\alpha}^i}{\bar{\alpha}^i\bar{\alpha}^j} + 0.11\dfrac{\bar{\mu}^{i2}\bar{\alpha}^j + \bar{\mu}^{j2}\bar{\alpha}^i}{\bar{\alpha}^i\bar{\alpha}^j}\right)^{-1} & \text{if } i \text{ and } j \notin DC_w \\ \left(1 + 0.25\bar{r}^{ij2}\dfrac{\bar{q}^{w2}}{\bar{\alpha}^w} + 0.11\dfrac{\bar{\mu}^{w2}}{\bar{\alpha}^w}\right)^{-1} \simeq 0.72 & \text{otherwise} \end{cases}
\quad (9)
$$

where DC_w is the group of DCs that belong to the already polarizable SWM4-NDP water molecules. Considering the dipole moment, molecular polarizability, and net charge of water molecules, $\bar{\mu}^w = 1.855\ D$ [45], $\bar{\alpha}^w = 0.97825\ Å^3$ [46], and $\bar{q}^w = 0$, Eq. 9 gives the scaling factor for ion-water interaction as $k_{LJ}^{ij} \simeq 0.72$.

In the present study, the Drude oscillator model is combined with both the non-polarizable and polarizable water models, as discussed later in Sec. 2.2.1, respectively coined as "partially" and "fully" polarizable force fields.

B. Maintaining simulation stability

Although Drude polarizable force fields are known for their feasible implementation, maintaining simulation stability along a long MD trajectory is a critical challenge when using such force fields. Particularly, in the presence of atoms with high atomic polarizabilities, such as the OTF⁻ in our

simulations, a DP can escape from its DC and be captured by another DC, which makes the force and energy diverge and the simulation crash. Furthermore, at short distances, the interactions between the induced dipoles become very strong, leading to exaggerated correlation between nearby dipoles, which is a known problem as "polarisation catastrophe" [47]. Therefore, to reduce the dipolar electrostatic interactions at short distances, the Thole damping function [47-48] is applied. For two polarizable atoms i and j, the damping function is given by

$$T^{ij}(r^{ij}) = 1 - \left(1 + \frac{s^{ij}r^{ij}}{2}\right)exp(-s^{ij}r^{ij}) \tag{10}$$

where the scaling parameter s^{ij} is determined by the atomic polarizabilities $\alpha^{i,j}$ and a damping parameter $a^{i,j}$

$$s^{ij} = \frac{a^i + a^j}{2(\alpha^i\alpha^j)^{1/6}} \tag{11}$$

The Thole damping function is only applied to the interactions between the point charges representing the induced dipoles on polarizable atoms, i.e., the charges on DPs, $-q_D^{i,j}$, and the opposite charges located on the respective DCs, $q_D^{i,j}$ (the latter is only part of the full charges of DCs).

In the presence of small highly charged atoms, such as Na^+, another damping function is required to adjust the short-range coulomb interactions between such atoms and the induced dipoles. For this purpose, we use a modified Tang-Toennies (TT) function [49], as proposed by Goloviznina et al.[50]

$$f_{TT}^{ij}(r^{ij}) = \begin{cases} 1 - c_{TT} \cdot e^{-b_{TT}r^{ij}} \sum_{k=0}^{4} \frac{(b_{TT}r^{ij})^k}{k!} & i \text{ or } j \in DC_{Na} \\ 1 & otherwise \end{cases} \tag{12}$$

where DC_{Na} denotes the group of DCs that belong to Na$^+$ ions and b_{TT} and c_{TT} adjust the interaction strength. The TT damping function is only applied to the interactions between the non-polarizable part

of the charges on the DCs of highly charged polarizable atoms (here, Na^+ ions), $q'^i = q^i - q_D^i$, and the

Drude charges on the DPs and DCs of the other polarizable atoms, $\pm q_D^j$ (see Eq. 13).

In addition to the above-mentioned stability issues, the flying ice cube artifact [51], i.e., irreversible transfer of linear momentum to the center of mass of the system, may also need to be avoided. This artifact can be identified by the unphysically fast change in the mean squared displacement of randomly walking atoms, which usually increases linearly with time. Although the flying ice cube is mostly reported for simulations where temperature is kept constant by velocity rescaling [51-53] (e.g., when the Berendsen thermostat is used), this situation may occur in the presence of Drude oscillators even when the Nose-Hoover thermostat is used. In this case, the problem occurs because the two separate thermostats applied to the atomic and dipolar subsystems (see Sec. 2.3, paragraph 2) are insensitive to how the kinetic energy is partitioned among the degrees of freedom [54]. As detailed in Ref. [54], it causes an accumulation of small numerical errors along MD trajectories and may give rise to the flying ice cube artifact at a certain point. In the presence of SWM4-NDP water molecules, this problem is more severe because another separate Nose-Hoover thermostat (with chains) must be applied to the rigid water molecules (see Sec. 2.3, paragraph 2). To avoid this problem, the linear momentum of the whole system should be zeroed by subtracting the center-of-mass velocity from the velocity of each atom every time step. In Sec. 3.5, we discuss more about this artifact and the simulation conditions under which the flying ice cube effect occurs.

C. Functional form of the potential energy

For the polarizable force field, considering the interactions associated with DPs and DCs, the non-bonded term of the potential energy is written as

$U_{non-bonded} =$

$$\sum_a \sum_{b>a} w^{ab} \left(4\varepsilon^{ab} \left[\left(\frac{\sigma^{ab}}{r^{ab}}\right)^{12} - \left(\frac{\sigma^{ab}}{r^{ab}}\right)^{6} \right] + \frac{q^a q^b}{4\pi\varepsilon_0 r^{ab}} \right)$$

$$+ \sum_k \sum_{s>k} w^{ks} \left(4k_{LJ}^{ks} \varepsilon^{ks} \left[\left(\frac{\sigma^{ks}}{r^{ks}}\right)^{12} - \left(\frac{\sigma^{ks}}{r^{ks}}\right)^{6} \right] \right. \tag{13}$$

$$\left. + \frac{(q^k - q_D^k)(q^s - q_D^s) + f_{TT}^{ks}(r^{ks})\left((q^k - q_D^k)q_D^s + q_D^k(q^s - q_D^s)\right) + T^{ks}(r^{ks})q_D^k q_D^s}{4\pi\varepsilon_0 r^{ks}} \right)$$

$$+ \sum_m \sum_{n>m} w^{mn} \left(\frac{T^{mn}(r^{mn})q^m q^n}{4\pi\varepsilon_0 r^{mn}} \right) + \sum_a \sum_k w^{ak} \left(4\varepsilon^{ak} \left[\left(\frac{\sigma^{ak}}{r^{ak}}\right)^{12} - \left(\frac{\sigma^{ak}}{r^{ak}}\right)^{6} \right] + \frac{q^a q^k}{4\pi\varepsilon_0 r^{ak}} \right)$$

$$+ \sum_a \sum_m w^{am} \left(\frac{q^a q^m}{4\pi\varepsilon_0 r^{am}} \right) + \sum_k \sum_m w^{km} \left(\frac{f_{TT}^{km}(r^{km})\left(q^k - q_D^k\right)q^m + T^{km}(r^{km})q_D^k q^m}{4\pi\varepsilon_0 r^{km}} \right)$$

where the indices a and b run over non-polarizable atoms (here, water oxygen and hydrogen), k and s run over DCs, and m and n run over DPs.

The bonded term of the potential energy, including the intramolecular interactions and the harmonic interactions between DPs and their respective DCs (see Eq. 6), can be written as

$$U_{bonded} = \sum_{ij \in bonds} k_b^{ij}\left(r^{ij} - r_0^{ij}\right)^2 + \sum_{ijk \in angles} k_\theta^{ijk}\left(\theta^{ijk} - \theta_0^{ijk}\right)^2$$

$$+ \sum_{\substack{ijks \in \\ dihedrals}} \sum_{m=1}^{4} \frac{k_m^{ijks}}{2}\left[1 + (-1)^{m+1}\cos\left(m\varphi_0^{ijks}\right)\right] + \sum_{n \in dipoles} \frac{k_D^n}{2} r_D^{n\,2} \tag{14}$$

with $dipoles$ being the group of DC-DP pairs representing the induced dipoles on polarizable sites.

2.2 Parameterization of the force field potential

In addition to the functional form of the potential, a force field requires a set of parameters that determine the physical and chemical properties. General force field parameters describe the types of atoms, chemical bonds, dihedral angles, out-of-plane interactions, and non-bonded interactions. Depending on

the employed methods, force fields may also include several specific parameters. For example, modelling of polarization via Drude oscillators introduces additional force field parameters that adjust Drude interactions. A crucial step in MD simulations is to parametrize the force field to represent the target system properly. Therefore, it is essential to investigate how the system properties are sensitive to the different force field parameters. In the present work, starting with a set of parameters that we refer to as the base set of force field parameters, we study the effect of different force field parameters on the properties of the studied WiS solution. The selected parameters are described as follows.

2.2.1 Water model

The ion solvation structure and other structural and physico-chemical properties of the electrolyte are sensitive to parameters used to model inter- and intramolecular interactions of water molecules. In this work, several water models are selected to probe the influence of water force field parameters. We start from the nono-polarizable models, i.e., the rigid 3-site models SPC, SPC/E, TIP3P, and OPC3, the flexible 3-site model SPC/Fw, and the rigid 4-site model TIP4P. Table 1 shows the parameters of the employed models. To hold the shape of water molecules in the rigid models in table 1, the SHAKE algorithm is applied. In our base non-polarizable and partially polarizable simulations (BNP and BPP force fields), we use the widely accepted SPC/E model.

In addition to the non-polarizable water models listed in table 1, we use the SWM4-NDP model that explicitly accounts for water polarization via Drude particles attached to water oxygens O_w. The SWM4-NDP model is known to provide a dielectric constant close to the experimental data, which makes it suitable for where water-mediated electrostatic interactions are important [55-56]. This model is a rigid 4-site model containing a massless site, M, which is restrained by a harmonic potential to O_w (see Fig. 1). The parameters of this model are given in table 2. Instead of using the SHAKE algorithm for geometry constraints, SWM4-NDP water molecules are simulated as rigid bodies that are integrated separately, as described in Sec. 2.3.

Table 1. Force field parameters for the non-polarizable water models examined in this work (in all models: $\sigma^H = \varepsilon^H = 0$)

	SPC [57]	SPC/Fw [58]	SPC/E [59]	TIP3P [60]	TIP4P [60]	OPC3 [61]
Type	3-site Rigid	3-site Flexible	3-site Rigid	3-site Rigid	4-site Rigid	3-site Rigid
q^O (e)	-0.82	-0.82	-0.8476	-0.830	-1.0484	-0.89517
q^H (e)	0.41	0.41	0.4238	0.415	0.5242	0.447585
σ^O (Å)	3.166	3.165	3.166	3.188	3.16435	3.17427
ε^O (kcal/mol)	0.15535	0.155	0.15535	0.102	0.16275	0.163406
r_0^{OH} (Å)	1.0	1.012	1.0	0.9572	0.957200	0.97888
k_b^{OH} (kcal/molÅ²)	–	529.581	–	–	–	–
θ_0^{HOH} (°)	109.47	113.24	109.47	104.52	104.52	109.47
k_θ^{HOH} (kcal/molrad²)	–	37.95	–	–	–	–
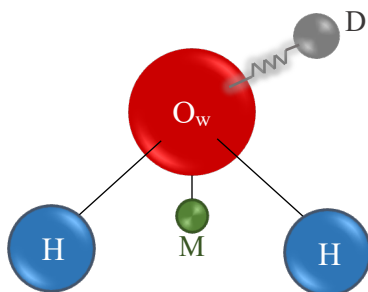
Figure 1. Schematic structure of a SWM4-NDP water molecule

Table 2. Force field parameters for the polarizable water model SWM4-NDP [46]

q^O (e)	q^H (e)	q^M (e)	q^D (e)	σ^O (Å)	ε^O (kcal/mol)	r^{OH} (Å)	r^{OM} (Å)	θ^{HOH} (°)	$k_D^{O_w}$ (kcal/molÅ²)
1.71636	0.55733	$-2q_H$	$-q_O$	3.18395	0.21094	0.9572	0.24034	104.52	1000

2.2.2 Ion parameters

We describe the interactions of monatomic ions (here, Na⁺) through the LJ parameters in Eq. 2 and the ionic charge scaling factor given by Eq. 3. For the LJ parameters of Na⁺, we use seven sets of ε^{Na} and σ^{Na} proposed in the literature (see table 3). The GROMOS parameters are used in our base non-polarizable, base partially polarizable, and fully polarizable simulations (BNP, BPP, and FP force fields).

For polyatomic ions (here, OTF⁻), in addition to the LJ parameters of the constituent atoms, their partial charges and the parameters for the bonded potentials in Eq. 5 are also necessary. In the present work, we take the force field parameters listed in table 4 for OTF⁻ anions from the literature [62-63].

Table 3. Lennard-Jones (LJ) interaction parameters for Na^+

	OPLS [64]	Cheatham [65-66]	Loche [67]	Roux [68]	GROMOS [69]	Aqvist [70]	Jorgensen [66, 71]
ε^{Na} (kcal/mol)	1.607139	0.352875	0.1075526	0.0469	0.0148	0.00277	0.0005
σ^{Na} (Å)	1.89744	2.1559	2.31	2.42993	2.58	3.33045	4.014

Table 4. Force field parameters for OTF⁻ [62]

Nonbonded parameters	Atom (i)	σ^i (Å)	ε^i (kcal/mol)	q^i (e)	α^i (Å³)*
	C	3.5	0.065999	0.35	0.982
	F	2.95	0.053	-0.16	0.604
	O	2.96	0.21	-0.63	1.114
	S	3.55	0.25	1.02	1.431
Internal stretching parameters	bond (ij)	r_0^{ij} (Å)	k_b^{i-j} (kcal/molÅ²)		
	C-F	1.323	441.8021		
	C-S	1.818	235.42065		
	S-O	1.442	637.069790		
Internal bending parameters	angle (ijk)	θ_0^{ijk} (°)	k_θ^{ijk} (kcal/molrad²)		
	F-C-F	107.1	93.33174		
	S-C-F	111.8	82.93499		
	C-S-O	102.6	103.9675		
	O-S-O	115.3	115.7983		
Dihedral parameters	Dihedral ($ijks$)	k_1^{ijks} (kcal/mol)	k_2^{ijks} (kcal/mol)	k_3^{ijks} (kcal/mol)	k_4^{ijks} (kcal/mol)
	F-C-S-O	0.0	0.0	0.34679	0.0

* Atomic polarizabilities are set according to Ref. [63] and are used only in the case of the polarizable force field

As discussed earlier, in non-polarizable force fields, electronic polarization can be accounted for in a mean-field way via ionic charge scaling (see Eqs. 2-3). Although a scaling factor of 0.7–0.8 is known to reproduce reasonable thermodynamic properties for ionic liquids [36], the optimal scaling factor is still in debate [35]. In the present study, the scaling factor k_q (see Eq. 3) is varied from 1 to 0.7 to address the effect of the charge scaling on the electrolyte properties. In our base non-polarizable (BNP) force field, we set $k_q = 1$. In the polarizable simulations, we do not apply a charge scaling factor.

2.2.3 Mass of the DPs

DPs must stay spatially close to their DC, which can be realized by a small particle mass and stiff harmonic bond. In all our simulations, the mass of all Drude particles is set to $m_D = 0.4 \ g/mol$, suggested by Lamoureux and Roux [54]. A smaller m_D requires a smaller time step and can affect the simulation stability.

2.2.4 DP-DC force constant k_D

As discussed earlier, a Drude particle is bound to its core atom by a harmonic force with a force constant of k_D that adjusts the charge of the Drude particle (see Eq. 7) and its displacement from the core atom. Lamoureux and Roux [54] suggested to use k_D= 1000 $kcal/mol \ \text{Å}^2$ for all types of DP-DC bonds. Heid et al. [72], however, reported that a higher force constant of $k_D = 2000 \ kcal/mol \ \text{Å}^2$ performs slightly better than $k_D = 1000 \ kcal/mol \ \text{Å}^2$, as it results in higher Drude charges which are closer to the core atoms. In the present work, we vary k_D from 1000 to 4000 $kcal/mol \ \text{Å}^2$ to investigate how this parameter affects the electrolyte properties. We note that for smaller values of k_D, the simulation becomes unstable. The standard value k_D= 2000 $kcal/mol \ \text{Å}^2$ is used in our BPP and FP force fields.

2.2.5 Atomic polarizabilities

Atomic polarizabilities not only determine the partial charges on Drude pairs, as given by Eq. 7, but also affect the scaling factors for LJ interactions of polarizable atoms, k_{LJ}^{ij} (see Eq. 8), and the Thole scaling parameters, S^{ij} (see Eq. 11). The measured and calculated values of the atomic polarizability can be various depending on the experimental and computational methods. In our BPP and FP force fields, the polarizability of Na$^+$ is set to $\alpha_{Na} = 0.157 \ \text{Å}^3$, which was originally calculated in the gaseous phase [73], but is widely used for various simulations of liquid solutions via classical Drude oscillators [74-77]. A range of α_{Na}, including five values reported in the literature (see table 5), are also used in our partially polarizable simulations to investigate how α_{Na} affects the electrolyte properties. The polarizabilities of

the atoms of OTF⁻ anions are set according to Ref. [63] in the BPP and FP force fields (see table 4) and uniformly scaled by a factor of $k_\alpha^{OTF} = 0.25 - 0.9$ in our partially polarizable simulations. It is worth noting that since the polarizability response to a small temperature variation is negligible, we use the polarizabilities measured at 25°C.

Table 5. Literature values of Na⁺ polarizability, α_{Na} (all values are in Å³)

Ref. [78]	Refs. [73-74]	Ref. [79]	Ref. [80]	Ref. [81]
0.12 [I]	0.157 [II]	0.18 [III]	0.24 [IV]	0.279 [V]

[I] from the Amoeba polarizable force field
[II] originally calculated in the gaseous phase, but widely used for the simulation of liquid solutions via Drude oscillators
[III] obtained from DFT calculations
[IV] used in DC97 force fields [79]
[V] calculated based on a theory that predicts a linear relationship between the refractive index of a salt solution and its salt concentration [81]

2.2.6 Thole damping parameter

The parameter a_i in Eq. 11, which adjusts the strength of the short-distance dipole-dipole interactions, usually takes a default value of 2.6 [82] (or 2.08 in the AMBER force field [47]) for all polarizable atoms. In certain force fields, the value may depend on the atom types [48]. In the present study, we use the same Thole damping parameter, a, for all polarizable particles, but the value of this parameter is varied to examine its effect on simulation results. In the BPP and FP force fields , this parameter is set to $a = 2.6$.

2.2.7 Tang-Toennies damping parameters

The parameters b_{TT} and c_{TT} in the TT damping function (Eq. 12) adjust the strength of the short-range interactions between DCs of Na⁺ atoms and all Drude pairs (both DCs and DPs). Goloviznina et al. [50] reported that the parameter b_{TT}=4.5 is optimal for the ionic liquids investigated in their work. They used c_{TT}=1 in their calculations, satisfying an asymptotic behavior $f_{TT}^{ij}(r^{ij}) \to 0$ when $r^{ij} \to 0$. We use the same parameters in our BPP and FP force fields . However, the parameters are tested at intervals where the simulation remains stable for partially polarizable simulations.

2.2.8 Base set of force field parameters

The parameter sets used in our base non-polarizable (BNP), base partially polarizable (BPP), and fully

polarizable (FP) force fields are summarized in table 6.

Table 6. The base set of parameters in our non-polarizable, partially polarizable, and fully polarizable
simulations

General force field parameters (for BNP, BPP, and FP simulations)	
Water model	SPC/E (see table 1) for the BNP and BPP force fields
	SWM4-NDP for the FP force field (see table 2)
Na^+ parameters	GROMOS (see table 3)
OTF^- parameters	according to Ref. [62] (see table 4)
Ionic charge scaling factor, K_q	1
Parameters that adjust Drude interactions (only for the BPP and FP force fields)	
Mass of the DPs, m_D	$0.4\ g/mol$
DP-DC force constant, k_D	$2000\ kcal/mol\ \text{Å}^2$
Polarizability of Na^+ ions, α^{Na}	$0.157\ \text{Å}^3$
Polarizability of the atoms of OTF^- anions	according to Ref. [63] (see table 4)
Thole damping parameter a (see Eq. 11)	2.6
TT damping parameter b_{TT} (see Eq. 12)	4.5
TT damping parameter c_{TT} (see Eq. 12)	1

2.3 Simulation setup

We use a cubic simulation box with initial dimensions of $28 \times 28 \times 28\ \text{Å}^3$ and periodic boundary

conditions in all three directions. 80 salt ion pairs and 480 water molecules are randomly distributed

within the simulation box, corresponding to a salt concentration of 9.25 m. The energy of the system is

minimized via the Polak-Ribiere version of the conjugate gradient (CG) method [83]. For polarizable

simulations, Drude particles are added to the energy minimized configuration using the polarizer tool,

which is distributed with the LAMMPS package and described in Ref. [84]. The initial velocity for each

atom is determined using a Gaussian distribution based on the specified temperature. For the long-range

Coulomb interactions, the P3M algorithm [85] is employed and tuned to obtain a maximum relative error

of 10^{-4} in the calculated forces. All simulations are performed in LAMMPS [86] using the velocity Verlet

method.

We statistically sample canonical NVT ensembles at 333 K using the Nose–Hoover thermostat with a relaxation time of 0.1 ps. For polarizable simulations, special treatment is required concerning the thermostat to keep the temperature of DPs low and ensure that Drude oscillations do not influence the kinetic energy of the atoms. For this purpose, a dual Nose-Hoover thermostat is used to maintain the Drude degrees of freedom at 1 K, which is small enough to leave almost no kinetic energy to the vibration of the Drude particles but large enough to respond to the room-temperature motions of the nuclei [72]. In the fully polarizable force field, i.e., when the SWM4-NDP water model is used, the rigid SWM4-NDP water molecules are also integrated separately using an independent Nose-Hoover thermostat (or barostat) with chains [87], which is applied to both the translational and rotational degrees of freedom of water molecules (for more details, see Ref. [88]). For thermalizing the Drude particles using a Nose-Hoover thermostat in the fully polarizable force field, the atomic masses, positions, velocities, and forces are converted into a reduced representation where the DCs transform into the centers of mass of the DC-DP pairs and the DPs transform into their relative positions with respect to their cores (see Ref. [54]).

All polarizable and non-polarizable simulations are performed in two steps. First, the pressure and volume of the system are equilibrated using a 2 ns simulation in an NPT ensemble utilizing a Nose-Hoover barostat with a target pressure of 1 atm and one or more Nose-Hoover thermostats (as described above) with a target temperature of 333 K. Subsequently, simulations are continued for 22 ns in the corresponding NVT ensemble, the last few nanoseconds of which are used to calculate the electrolyte properties, as described in Sec. 2.4. For non-polarizable simulations, the time step is set to 2 fs. The time step for polarizable simulations is set to 0.1-0.5 fs to make the simulations stable (simulation stability is discussed in detail later). All simulations are carried out on 24-48 CPU cores.

2.4 Sampling and analysis methods of electrolyte properties

In the following, the numerical analysis for the different electrolyte properties is briefly described.

2.4.1 Diffusion coefficient

The random Brownian motion of particles diffusing in a liquid is well described by the Einstein relation

$$\langle |r(t) - r(0)|^2 \rangle = 2nDt \tag{15}$$

where $\langle |r(t) - r(0)|^2 \rangle$ is the mean squared displacement (MSD), n is the number of dimensions being considered (here, $n = 3$), D is the diffusion coefficient, and t is time. According to Eq. 15, for sufficient statistical sampling, the slope of the linear fit to MSD versus time converges to $2nD$, from which the diffusion coefficient can be determined. In addition to a large enough sampling time, a sufficient number of diffusing particles is required to obtain a reliable diffusion coefficient. But in most of molecular dynamics simulation methods, there are computational limitations on the number of particles and simulation time, leading to fluctuations in this curve. The fluctuations can be efficiently reduced by averaging the mean squared displacements obtained from either different trajectories with different reference positions or different segments of a long enough trajectory. In the present study, the last 20 ns of the trajectories are broken to 10 segments of equal length and $MSD(t)$ is averaged over all segments. We use this method to calculate the diffusion coefficient of cations in the studied WiS solution, which is of paramount importance in ion battery simulations.

An important point to note here is that although Ab initio molecular dynamics (AIMD) simulations are much more accurate than classical MD simulations, in many cases they are not suitable for the calculation of the diffusion coefficient from Eq. 15. The reason is that AIMD is computationally demanding and thus can be applied only to small systems over short periods of time (of tens of picoseconds). It makes it difficult to exclude the correlation effect in the MSD versus time plot due to insufficient sampling, which can increase the error in the calculation of the diffusion coefficient.

2.4.2 Viscosity

We extract the viscosity of the studied bulk WiS electrolyte from the off-diagonal components of the Green–Kubo expression

$$\eta = \frac{V}{10k_BT} \int_0^\infty \left\langle \sum_{\alpha\beta} P_{\alpha\beta}(\tau + \tau_0) P_{\alpha\beta}(\tau_0) \right\rangle_{\tau_0} d\tau \tag{16}$$

with V being the volume of the simulation box and $P_{\alpha\beta}(\tau)$ being the stress in the $\alpha\beta$ plane as a function of time. In all our simulations, the last 2.5-5 ns of the production run is used to calculate the viscosity from Eq. 16.

2.4.3 Structural properties

To investigate how the solution structure depends on the force field parameters, the radial pair distribution function (RDF) is calculated for different atom pairs from

$$g(r) = \frac{\rho(r)}{\rho_{bulk}} \tag{17}$$

with r being the distance from the central atom and $\rho(r)$ and ρ_{bulk} being the local and bulk densities of the other atom, respectively. We define the positions of the first peaks in RDFs as the equilibrium distances between the corresponding atom pairs. Also, the first and the second minimums in the Na-O$_w$ RDF are considered as the boundaries of the first and the second solvation shells around Na$^+$, respectively. The coordination number (CN) of Na$^+$ is the number of water (or OTF$^-$) molecules up to the boundary of its first solvation shell. Based on the number of the anions located within the first and second solvation shells of Na$^+$, solvation structure is categorized into four kinds: free Na$^+$ ions that have no anions in their first and second solvation shells, solvent-separated ion pairs (SSIPs), where at least one anion resides in the second solvation shell of Na$^+$ while the first shell is free of anions, contact ion pairs (CIPs), with one anion located in the first solvation shell of Na$^+$, and aggregating ion pairs (AGGs), containing more than one anion in the first solvation shell around Na$^+$. To examine the solvation structures in the studied WiS solution, the number of the anions residing within the two solvation shells

of each Na^+ atom is calculated every 50 ps from the last 5 ns of the production run. The results are then averaged over time and used to calculate the proportion of the different solvation structures.

2.4.4 Vibrational frequencies

To calculate the vibrational frequencies, the last 25 ps of the simulation trajectories are broken to 10 segments of equal length and the velocity auto-correlation function (VACF) vs. time is calculated for each segment and averaged over all segments. This is done separately for water and ions, i.e., the VACF is averaged once over water molecules and once over Na^+ and OTF^- ions. Then, a one-dimensional discrete Fourier Transform is applied to VACF, characterizing the vibrational spectra of water and ions.

3 Results and discussion

Now, we present the properties of the studied WiS electrolyte and their sensitivity to the force field parameters by performing classical MD simulations using both non-polarizable forcefields (with and without scaling the ionic charges) and Drude polarizable force fields (with and without explicit modeling of water polarizability), as described in section 2.1.

3.1 Non-polarizable force field

For the non-polarizable force field described in section 2.1.1, we start from a base set of parameters, listed in table 5, and vary the parameters that adjust the inter- and intramolecular interactions.

In the first step, water force field is parameterized using the models described in table 1. Fig. 2a-f demonstrates the sampled properties of the WiS electrolyte. We note that all seven water models produce similar electrolyte properties in terms of the radial pair distribution functions (see panels a-d), the coordination environment of cations (see panel e), and the proportions of the different solvation structures: free ions, SSIPs, CIPs, and AGGs (see panel f). This indicates that the water models have only a minor effect on the microscopic structure of the WiS electrolyte. Furthermore, all water force field models predict almost the same vibrational frequencies (see Fig. 2g). However, the rigid models are not

able to capture the O_w-H stretch and H-O_w-H bending motions (see Fig. 2g, inset) because they treat fixed water configuration. The choice of the water model influences the diffusion coefficient of Na^+ more significantly. Among the studied models, OPC3 and TIP3P estimate the smallest and the largest diffusion coefficients for Na^+, respectively (see Fig. 2h). This can be attributed to the higher viscosity of the electrolyte in the presence of OPC3 water molecules than TIP3P molecules (see Fig. 2h). However, the dependence of the viscosity and the diffusion coefficient on the water parameters is weak, especially for SPC/E, TIP4P and OPC3 models, which are known as the most accurate non-polarizable water models for the bulk aqueous electrolytes. Thus, although the water model is a key factor determining the properties of aqueous electrolytes, the quality of the WiS electrolyte simulations has no significant dependence on the water models. In our following simulations, therefore, we use the SPC/E water model.
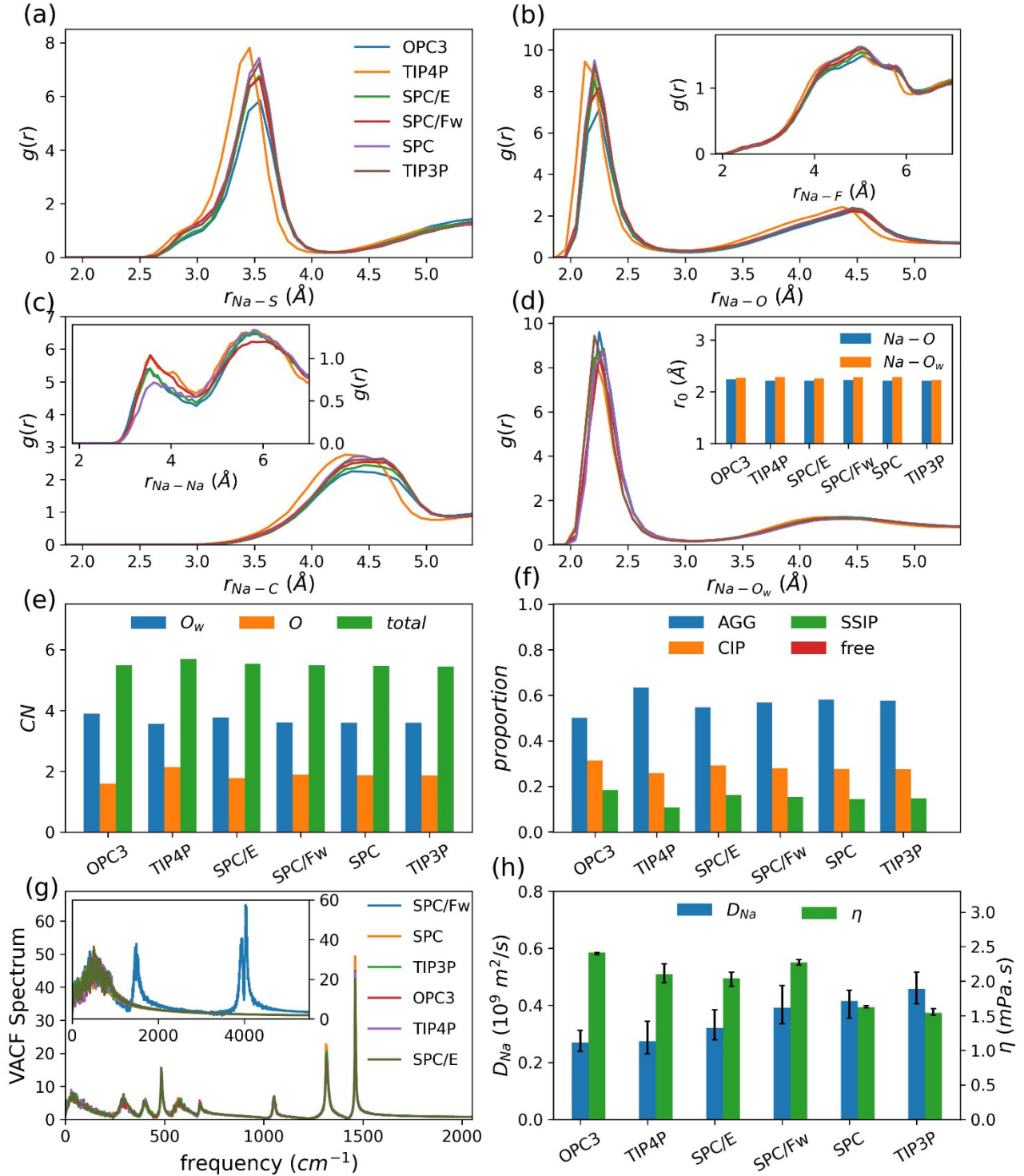
Figure 2. Effects of water model on the properties of the studied WiS electrolyte (results are obtained using the base non-polarizable force field described in table 6): (a-d) Radial pair distribution functions (RDFs) of the Na-S, Na-O, Na-F, Na-C, Na-Na, and Na-O_w pairs. The inset of panel (d) shows the positions of the first peaks in the Na-O and Na-O_w RDFs. (e) Total coordination number (CN) of Na$^+$ ions and the average number of the Na-coordinated O_w and O atoms. (f) Proportions of the solvation

structures described in section 2.4.3 (AGG: aggregates, CIP: contact ion pairs, SSIP: solvent-separated ion pairs, and free: free ions). (g) Vibrational spectra of ions (main panel) and water (inset). (h) Diffusion coefficient of Na^+ ions, D_{Na}, and viscosity of the electrolyte, η, in the various water models.

Next, using the LJ parameters for Na^+ listed in table 3, we investigate the influence of the size and short-range VdW interactions of cations. We note that, depending on the values set for σ^{Na} and ε^{Na}, the Na-S RDF shows one or two distinct peaks (see Fig. 3a), indicating that the Na-OTF coordination configuration is sensitive to these parameters. As shown schematically in the inset of Fig. 3a, OTF$^-$ can coordinate with Na^+ either monodentately, i.e., with one O atom bound to Na^+ , or bidentately, i.e., with two O atoms bound to Na^+ . In the monodentate configuration, the distance between Na^+ and S can be split by the bridging O atom as $r_0^{Na-S} \simeq r_0^{Na-O} + r_0^{O-S}$, with r_0^{Na-O} being the average distance between Na^+ and its neighbouring O atom (i.e., the position of the first peak in the Na-O RDF) and r_0^{O-S} being the optimal length of the O-S bond, $r_0^{O-S} = 1.442$ Å (see table 4). Therefore, the peak appearing in the Na-S RDF at $r_0^{Na-O} + r_0^{O-S}$ (here, around 3.5-3.75 Å) represents the monodentately Na-coordinated anion configurations. In the bidentate configuration, Na^+ gets closer to the S atom of its coordinated OTF$^-$ than in the monodentate configuration (see Fig. 3a, inset). Thus, the bidentately Na-coordinated anion configurations can be recognized by a peak appearing in the Na-S RDF at $r^{Na-S} < r_0^{Na-O} + r_0^{O-S}$. Accordingly, Fig. 3a shows that in all simulations, the monodentate coordination configuration is present, but the existence of bidentately coordinated ion pairs strongly depends on the LJ parameters of Na^+. In practice, the coordination configuration of a Na^+ cation and an OTF$^-$ anion is determined by the balance between the attractive LJ and repulsive coulomb contributions to the non-bonded interaction potential. Since the Na-S distance in the bidentate configuration is shorter than in the monodentate one, the repulsive coulomb force between Na^+ and the positively charged S atom is stronger for bidentately coordinated ion pairs. The bidentate configuration is, therefore, less stable than the monodentate one and accounts for a smaller proportion of ion pairs (see Fig. 3a). However, stronger attractive LJ interactions

between Na⁺ and OTF⁻, e.g., using the OPLS parameters for Na⁺, increase the occurrence of the bidentate configurations (see Fig. 3a).

We note that the average distance between Na⁺ ions and their neighbouring O atoms, r_0^{Na-O}, is influenced by the occurrence of bidentate configurations as well as the LJ interactions of Na⁺. When moving from the left column to the right of table 3, the LJ parameter sets represent a larger σ^{Na} and a smaller ε^{Na}, which correspond to a larger size and a weaker VdW attraction of Na⁺ ions, respectively. Supposedly, this increases the average distance between Na⁺ and its neighboring atoms. The inset of Fig. 3d, however, indicates a non-monotonic dependence of r_0^{Na-O} on the LJ parameters of Na⁺ (see Fig. 3d, inset). This is where the role of ion pair configuration comes into play. We note that the optimal Na-O distance for the bidentate pair configuration is slightly larger than for the monodentate one. For weaker LJ interactions, e.g. when using the Jorgensen LJ parameters for Na⁺, the ion pair configurations become less stable, resulting in a reduced occurrence of the bidentate configuration. This effect, which is manifested in the reduced hight of the peak appearing in the Na-S RDF at $r^{Na-S} < r_0^{Na-O} + r_0^{O-S}$ (see Fig. 3a), tends to decrease the average distance between Na⁺ ions and their neighbouring O atoms. When the electrolyte contains both the monodentate and bidentate Na-OTF configurations, the effect of the ion pair configuration is dominant, hence r_0^{Na-O} is inversely related to the strength of the LJ interactions of Na⁺ ions (see Figs. 3a and ad, inset). When the proportion of bidentate configurations is negligible, i.e., for GROMOS, Aqvist, and Jorgensen LJ parameters (see Fig. 3a), this effect disappears. In such a case, the LJ parameters corresponding to larger size and weaker LJ interactions of Na⁺ lead to larger values of r_0^{Na-O} (see Fig. 3d, inset), as expected. The inset of Fig. 3d indicates similar variations for the average distance between Na⁺ ions and their nearby water molecules, $r_0^{Na-O_w}$, which can be attributed to the pair coordination configuration dependence of the solvation structure around ion pairs.

According to Fig. 3e, all the LJ parameters studied here provide almost the same total coordination number of $CN \simeq 6$ for Na⁺ ions. However, the LJ parameter sets representing larger Na⁺ ions with weaker

VdW interactions provide smaller Na-OTF coordination numbers (see Fig. 3e). This indicates a higher degree of salt dissociation, which manifests itself in an increased proportion of CIPs and SSIPs at the expense of the proportion of AGGs (see Fig. 3f). Considering that the aggregated ion pairs diffuse together as a complex, the reduced proportion of AGGs indicates a decrease in the average size of the diffusing species. This factor, in addition to the weaker VdW interactions of Na^+ ions, causes a significant increase in the Na^+ diffusion coefficient, as shown in Fig. 3h. For example, the Na^+ diffusion coefficient obtained using the Jorgensen parameters is more than 10 times larger than that obtained using the OPLS parameters. Appropriate optimizations of the LJ parameters used for cations is, therefore, a crucial step in molecular dynamics modelling of WiS solutions, which has a major impact on both the structure and dynamics of the solution.

Fig. 3h gives a rough idea of how fast ions can diffuse in a WiS electrolyte. In the previous simulations of the monatomic ions Li^+, Na^+, and K^+, the LJ parameters typically follow the orders $\sigma_{Li^+} < \sigma_{Na^+} < \sigma_{K^+}$ and $\varepsilon_{Li^+} > \varepsilon_{Na^+} > \varepsilon_{K^+}$ [89, 90], which is similar to the variations followed by the LJ parameters listed in Table 3. Fig. 3h, therefore, indirectly indicates a relationship between the size of these ions and their diffusivity in the WiS electrolyte, $D_{Li^+} < D_{Na^+} < D_{K^+}$, as reported for Salt-in-Water solutions [74, 91-92]. For a more accurate assessment, of course, the force field parameters should first be optimized for each ion species.
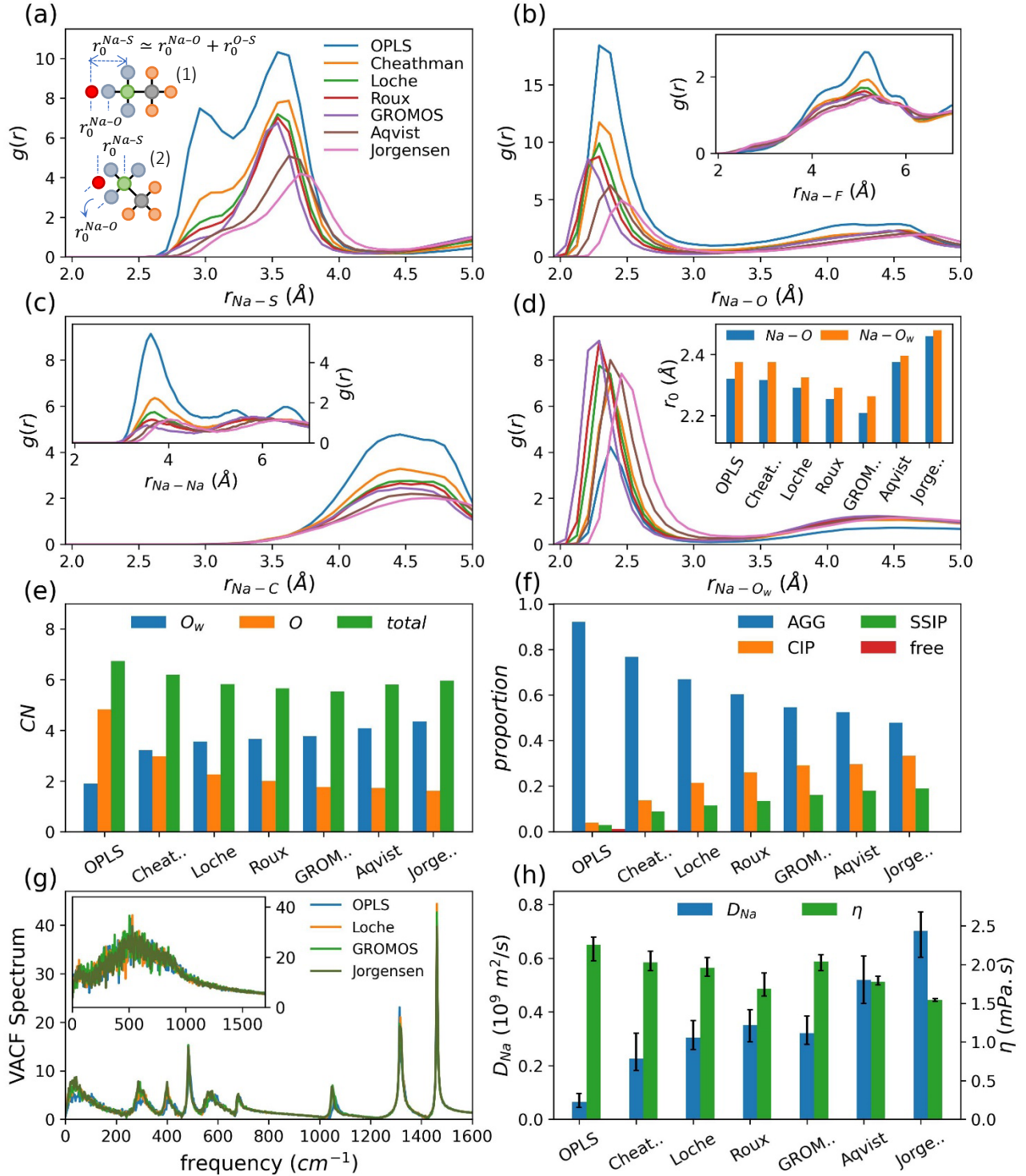
Figure 3. Dependence of the electrolyte properties on the Lennard-Jones (LJ) parameters for Na⁺ ions (the LJ parameters used for Na⁺ are given in table 2 and the other force field parameters are set according to the base non-polarizable force field described in table 6): (a-d) Radial pair distribution functions (RDFs) of the Na-S, Na-O, Na-F, Na-C, Na-Na, and Na-O_w pairs. The inset of panel (a) represents a schematic view of the (1) monodentate and (2) bidentate coordination configurations of OTF⁻ and Na⁺

pairs (Na, O, S, C, and F atoms are shown by red, blue, green, gray, and orange balls, respectively). The inset of panel (d) shows the positions of the first peaks in the Na-O and Na-O$_w$ RDFs. (e) Total coordination number (CN) of Na$^+$ ions and the average number of the Na-coordinated O$_w$ and O atoms. (f) Proportions of the solvation structures described in section 2.4.3 (AGG: aggregates, CIP: contact ion pairs, SSIP: solvent-separated ion pairs, and free: free ions). (g) Vibrational spectra of ions (main panel) and water (inset). (h) Diffusion coefficient of Na$^+$ ions, D_{Na}, and viscosity of the electrolyte, η, obtained using various LJ parameters for Na$^+$.

3.2 Uniform ion charge scaling in non-polarizable force fields

Based on a mean-field approach, the ionic charge scaling using factor k_q in Eq. 3 can account for the effective polarization within non-polarizable force field methods. Fig. 4a,b indicates that applying ionic charge scaling leads to a more disordered solvation shell around Na$^+$, which is manifested in the widening and lowering of the first peaks in the Na-O and Na-O$_w$ RDFs. However, the ionic charge scaling has only a minor effect on the other properties of the solvation structure, such as the equilibrium distance between Na$^+$ and its nearest atoms: O and O$_w$ (see Fig. 4b, inset), the coordination number of Na$^+$ (see Fig. 4c), and the Na-OTF pair configurations (see Fig. 4a, inset and the discussion in section 3.1). Furthermore, the ionic charge scaling slightly enhances the salt dissociation, leading to a gentle increase in the proportion of CIPs and SSIPs at the expense of the proportion of AGGs, while the number of free cations remains almost zero (see Fig. 4c, inset). In contrast, the dynamic properties of the solution are significantly dependent on the charge scaling factor. As shown in Fig. 4d, the viscosity of the solution decreases with decreasing the scaling factor due to the reduced ion-ion and ion-water electrostatic interactions. The decreased viscosity in addition to the reduced number of aggregates results in faster diffusion of Na$^+$ ions (Fig. 4d). As a result, the ionic charge scaling can be useful when the simulation calculates a lower diffusion rate than what is expected while the solvation structure does not need further adjustments. Fig. 5 shows the results obtained using three force field parameter sets listed in table 7, where the ionic charge scaling factor is adjusted to yield the same diffusion coefficients of $D_{Na} \simeq$

$0.36 \times 10^{-9} m^2/s$. This figure clearly shows that although these force field parameters provide the same diffusion coefficients for Na$^+$, they lead to completely different solvation structures around Na$^+$ and even different viscosities. The reduced number of AGGs in Sys. 3 (see Fig. 5c, inset) shows a higher degree of salt dissociation, which tends to increase D_{Na}. At the same time, however, it leads to an increase in viscosity of the solution (fig. 5d) due to the reduced number of uncoordinated water molecules (see Fig. 4c), which tends to decrease D_{Na}. The compensating contributions of these two factors result in the constant D_{Na}.
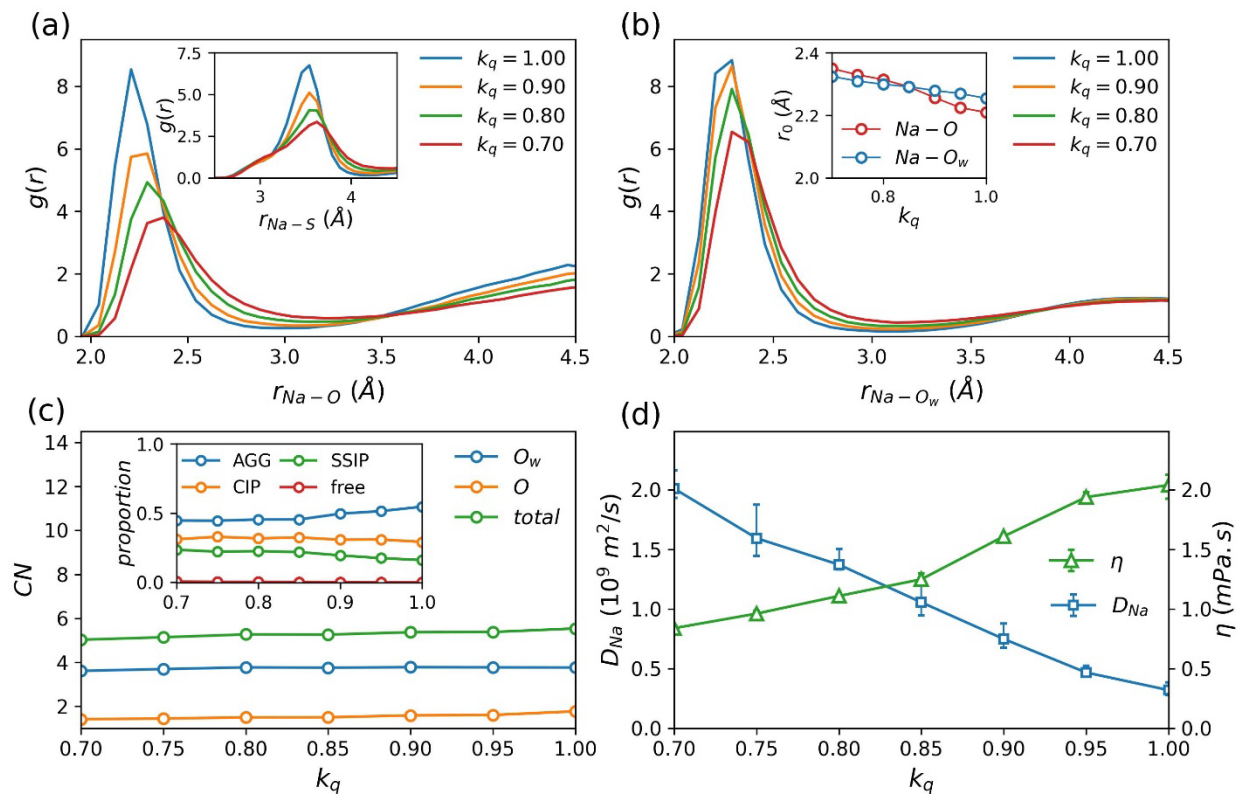

Figure 4. Effects of ionic charge scaling on the properties of the studied WiS electrolyte (results are obtained using the base non-polarizable force field described in table 6): (a, b) Radial pair distribution functions (RDFs) of the Na-O, Na-S, and Na-O$_w$ pairs. The inset of panel (b) shows the positions of the first peaks in the Na-O and Na-O$_w$ RDFs as a function of the charge scaling factor, k_q (see Eqs. 2 and 3). (c) Total coordination number (CN) of Na$^+$ and the average number of the Na-coordinated O$_w$ and O atoms as a function of k_q. The inset shows the proportion of different solvation structures vs. k_q (AGG: aggregates, CIP: contact ion pairs, SSIP: solvent-separated ion pairs, and free: free ions). (d) Diffusion coefficient of Na$^+$, D_{Na}, and viscosity of the electrolyte, η, as a function of k_q.

Table 7. Simulations with uniformly scaled ionic charges that predict the same Na diffusion coefficients of $D_{Na} = 0.36 \text{Å}^3$

	water model	LJ parameters for Na$^+$	scaling factor
Sys. 1	SPC/E	OPLS	0.800
Sys. 2	SPC/E	Cheathman	0.950
Sys. 3	OPC3	GROMOS	0.970
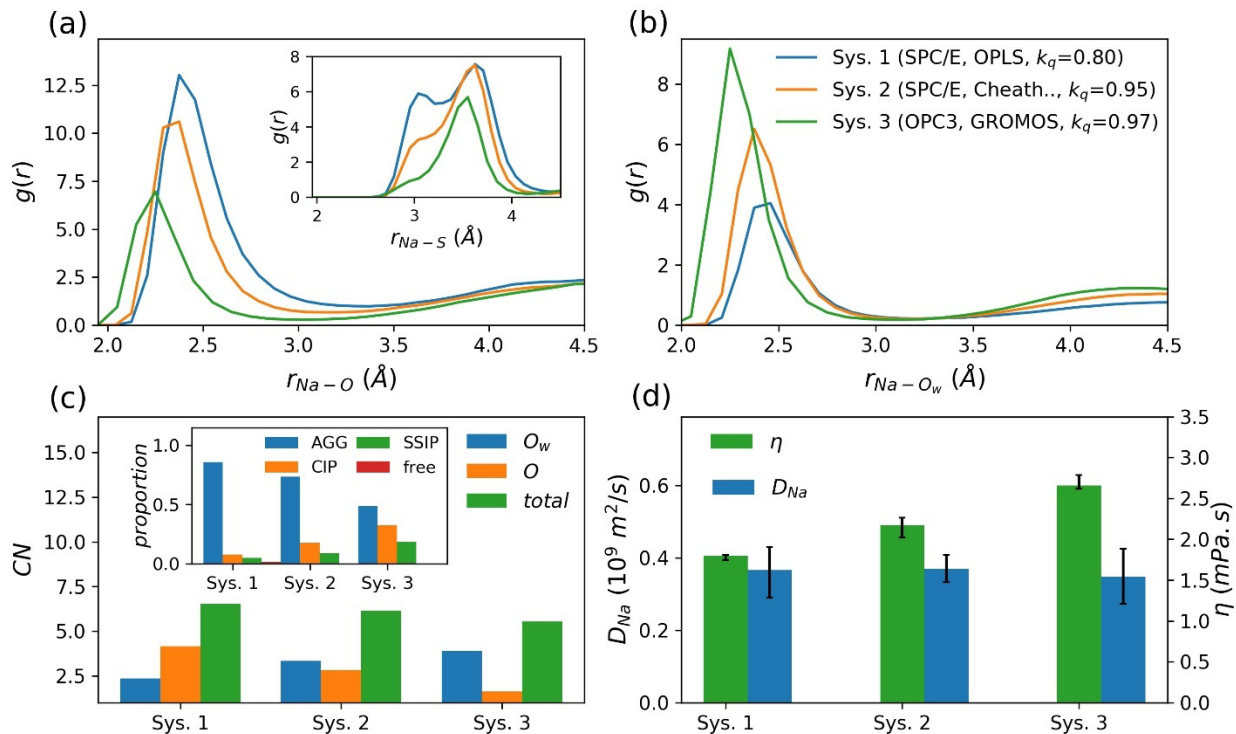
Figure 5. Properties of the studied WiS electrolyte obtained using the non-polarizable force field with the different force field parameters given in table 7, where the charge scaling factor, k_q (see Eqs. 2 and 3), is adjusted such that all simulations give the same diffusion coefficients: (a, b) Radial pair distribution functions (RDFs) of the Na-O, Na-S, and Na-O$_w$ pairs. (c) Total coordination number (CN) of Na$^+$ and the average number of the Na-coordinated O$_w$ and O atoms. The inset shows the proportions of different solvation structures (AGG: aggregates, CIP: contact ion pairs, SSIP: solvent-separated ion pairs, and free: free ions). (d) Diffusion coefficient of Na$^+$, D_{Na}, and viscosity of the electrolyte, η, for the studied systems.
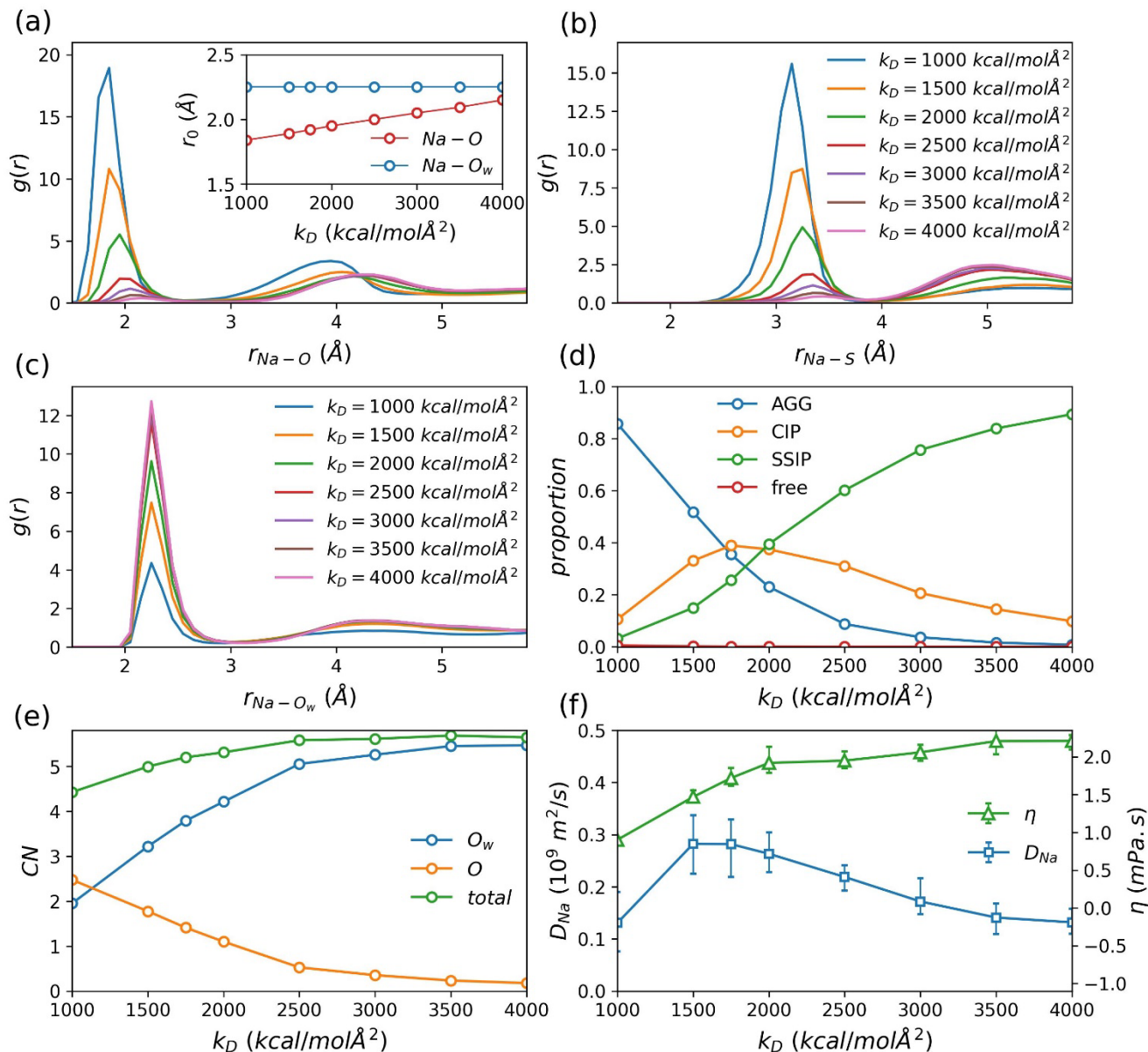
3.3 Partially Polarizable force field

As detailed in Sec. 2.1.2, the dynamic polarization is modeled explicitly using Drude oscillators. First, Drude particles are attached to Na$^+$ and the atoms of OTF$^-$ while water molecules are modeled using the

non-polarizable SPC/E model (the effect of water polarization is discussed later). The resulting force field is reffered to as a partially polarizable force field. We start with a base set of force field parameters, reffered to as the BPP force field (see table 6), and vary the parameters k_D, α_{Na}, b_{TT}, c_{TT}, k_α^{OTF}, and a that adjust Drude interactions (see sections 2.2.4-7) to investigate their effects on the electrolyte properties. Panel b in Figs. 6-11 show that all the studied Drude parameters predict a dominant monodentate Na-OTF coordination (see the discussion in Sec. 3.1), indicating that Drude parameters have no influence on the coordination configuration of Na-OTF ion pairs. The equilibrium distance between Na$^+$ and its nearest water molecules, $r_0^{Na-O_w}$, is also almost independent of the studied Drude parameters (see Figs. 6-11, the inset of panel a). The equilibrium distance between Na$^+$ and O atoms of OTF$^-$ anions, r_0^{Na-O}, however, increases with decreasing b_{TT} or with increasing either k_D, α^{Na}, or c_{TT} (see Fig. 6-11, the inset of panel a). Furthermore, the number of the Na-coordinated atoms, the proportion of different solvation structures, and the dynamic properties of the electrolyte are strongly dependent on the Drude parameters (see Figs. 6-11, panels d-f). Our results indicate that increasing b_{TT} or decreasing either α^{Na}, α^{OTF}, k_D, or c_{TT} causes a reduction in the proportion of SSIPs (see Figs. 6-11, panel d) and an increase in the number of Na-coordinated OTF$^-$ anions (see Figs. 6-11, panel e), while both the water coordination to Na$^+$ and the total coordination number of Na$^+$ decrease (see Figs. 6-11, panel e). In the absence of free Na$^+$ ions, this corresponds to a reduction in the NaOTF dissociation degree. For small enough values of b_{TT} or large enough values of either α^{Na}, α^{OTF}, k_D, or c_{TT}, all ion pairs are solvent-separated (fully dissociated salt) and the Na-water coordination number is around 5.6 (see Figs. 6-11, panels d and e), which is close to what ab initio MD simulations predict at the same temperature at low salt concentrations [93]. With a decrease in the degree of salt dissociation due to the above-mentioned variations in the Drude parameters, the proportion of AGGs increases monotonically, but the proportion of CIPs first increases and then starts to decrease (see Figs. 6-11, panel d). The reason is that the dissociation occurs from AGG to SSIP configurations through CIP, and the conversion from CIP to SSIP occurs faster than AGG to CIP at the parameters leading to a higher dissociation degree.

According to Figs. 6-11, panels d and f, at a higher degree of salt dissociation, the electrolyte shows a higher viscosity, which can be attributed to the reduced number of uncoordinated water molecules and the more dispersed charged species [94]. The degree of salt dissociation is more complicatedly related to ion diffusivity. The dissociation of ions decreases the number of ions that aggregate, which tends to increase ion diffusivity, but increases the viscosity (as discussed above), which tends to decrease ion diffusivity. These two competing factors cause non-monotonic variations in D_{Na}, as observed in Figs. 6-11, panel f. At low degrees of salt dissociation, where the AGG configuration is dominant, D_{Na} increases with any change in Drude parameters that increases the degree of salt dissociation, even though the solution becomes more viscous (see Figs. 6-11, panels d and f). In this case, the effect of the reduced size of the aggregates predominates. At higher degrees of salt dissociation, where the SSIP configuration prevails, however, D_{Na} decreases with the same changes in the Drude parameters (see Figs. 6-11, panels d and f), meaning that the effect of the increased viscosity becomes dominant. Panels d and f of Figs. 6-11 indicate that the Na$^+$ diffusivity is largest when SSIPs and AGGs have almost equal proportions of around 0.3 while the proportion of CIPs is at its maximum, i.e., at around 0.4. Close to the lower or upper edges of the studied Drude parameter range, i.e., when the ions are either fully associated or fully dissociated (see Figs. 6-11, panel d), the solvation structure and, consequently, both D_{Na} and η do not show significant changes with Drude patrameters (see Figs. 6-11, panel d-f). The only exception is a large viscosity change at small α^{Na} (see panel f of Fig. 7), which can be attributed to the changes in the number of Na-coordinated anions (see panel e of Fig. 7).

Among the studied Drude parameters, k_D, α^{Na}, b_{TT}, and c_{TT} have more pronounced effects on the electrolyte properties (see Figs. 6-9) and are therefore suitable for use in force field optimization. Although the anion polarizability influences the structure and viscosity of the electrolyte (see Fig. 10a-e), this parameter has a minor effect on the diffusion coefficient of cations (see Fig. 10f). Therefore, scaling the polarizabilities of anions is only worthwhile if the solution structure needs to be slightly modified, while maintaining the diffusion coefficient for cations. To simplify the force field optimization

process, however, the scaling of anion polarizability can be safely ignored. The Thole damping parameter a, which is allowed to vary in a small range of 2.1-2.8 due to the simulation stability problems, has only a minor effect on the electrolyte properties (see Fig. 11). This parameter, therefore, can be set to its standard value of 2.6 for most of the cases.
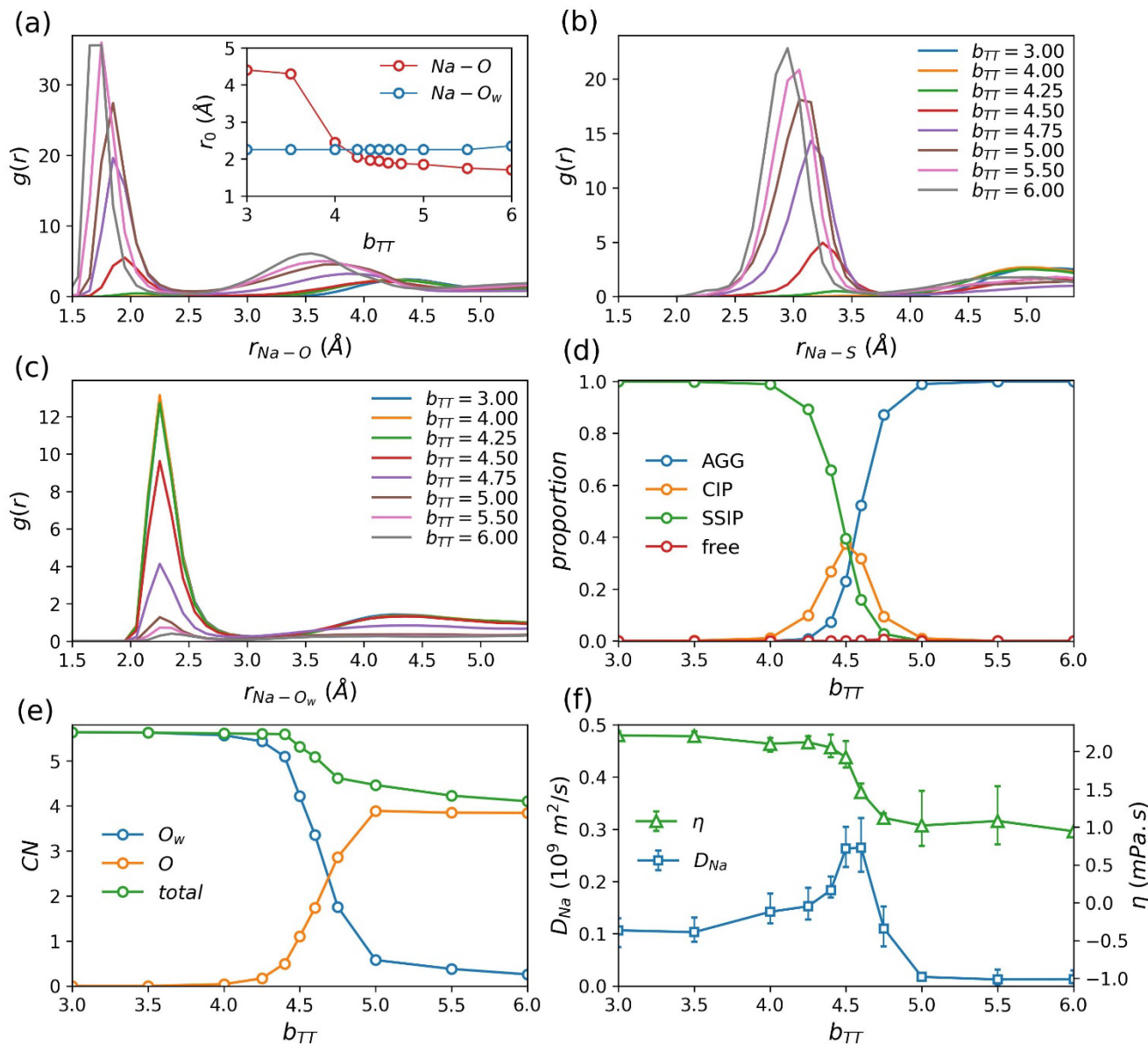

Figure 6. Dependence of the electrolyte properties on the harmonic spring force constant between Drude cores and Drude particles, k_D (other force field parameters are set according to the base polarizable force field described in table 6): (a-c) Radial pair distribution functions (RDFs) of the Na-O, Na-S, and Na-O$_w$ pairs. The inset shows the positions of the first peaks in the Na-O and Na-O$_w$ RDFs as a function of k_D. (d) Total coordination number (CN) of Na$^+$ and the average number of the Na-coordinated O$_w$ and O

atoms vs. k_D. (e) Proportions of different solvation structures as a function of k_D (AGG: aggregates, CIP: contact ion pairs, SSIP: solvent-separated ion pairs, and free: free ions). (f) Variation of the diffusion coefficient of Na$^+$, D_{Na}, and the viscosity of the electrolyte, η, with k_D.
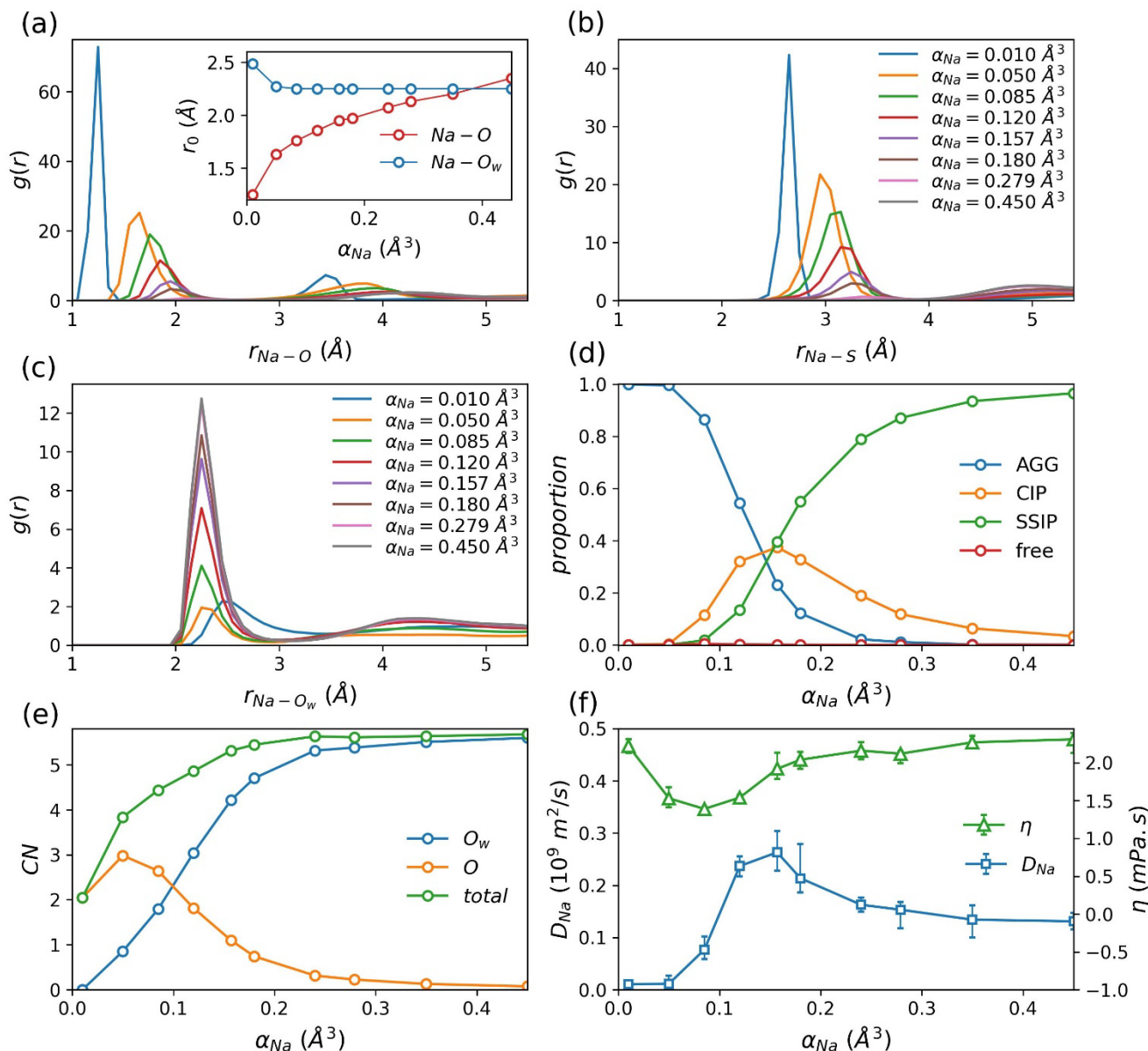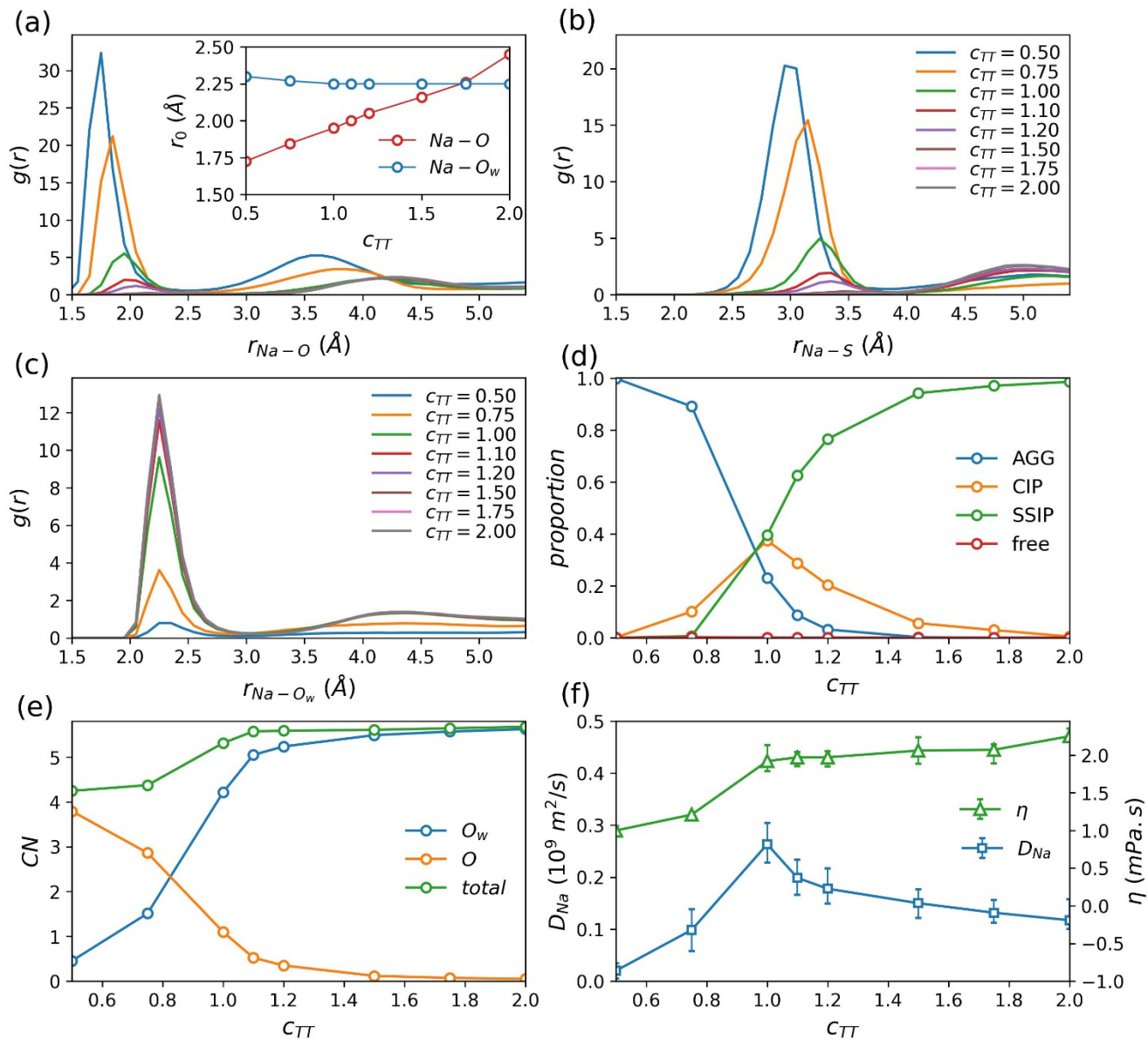

Figure 7. Dependence of the electrolyte properties on the polarizability of Na$^+$ ions, α^{Na} (other force field parameters are set according to the base polarizable force field described in table 6): (a-c) Radial pair distribution functions (RDFs) of the Na-O, Na-S, and Na-O$_w$ pairs. The inset shows the positions of the first peaks in the Na-O and Na-O$_w$ RDFs as a function of α^{Na}. (d) Total coordination number (CN) of Na$^+$ and the average number of the Na-coordinated O$_w$ and O atoms vs. α^{Na}. (e) Proportions of different solvation structures as a function of α^{Na} (AGG: aggregates, CIP: contact ion pairs, SSIP:

solvent-separated ion pairs, and free: free ions). (f) Diffusion coefficient of Na$^+$, D_{Na}, and viscosity of the electrolyte, η, as a function of α^{Na}.

Figure 8. Dependence of the electrolyte properties on the damping parameter b_{TT}, which is used in the Tang-Toennies function given by Eq. 12 (other force field parameters are set according to the base polarizable force field described in table 6): (a-c) Radial pair distribution functions (RDFs) of the Na-O, Na-S, and Na-O$_w$ pairs. The inset shows the positions of the first peaks in the Na-O and Na-O$_w$ RDFs as a function of b_{TT}. (d) Total coordination number (CN) of Na$^+$ and the average number of the Na-coordinated O$_w$ and O atoms vs. b_{TT}. (e) Proportions of different solvation structures as a function of b_{TT} (AGG: aggregates, CIP: contact ion pairs, SSIP: solvent-separated ion pairs, and free: free ions). (f) Diffusion coefficient of Na$^+$, D_{Na}, and viscosity of the electrolyte, η, as a function of b_{TT}.
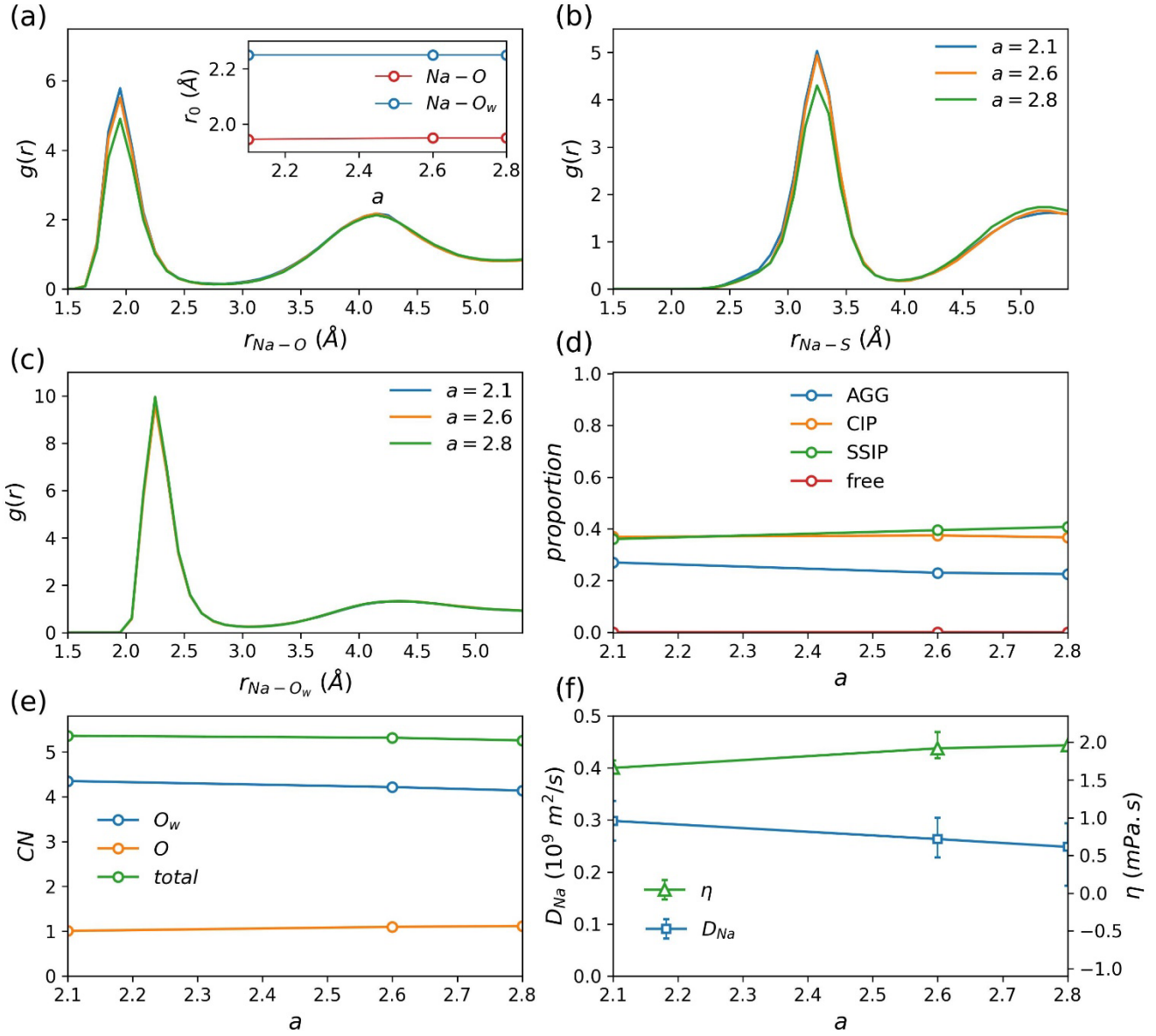
Figure 9. Variation of the electrolyte properties with the damping parameter c_{TT}, which is used in the Tang-Toennies function given by Eq. 12 (other force field parameters are set according to the base polarizable force field described in table 6): (a-c) Radial pair distribution functions (RDFs) of the Na-O, Na-S, and Na-O$_w$ pairs. The inset shows the positions of the first peaks in the Na-O and Na-O$_w$ RDFs as a function of c_{TT}. (d) Total coordination number (CN) of Na$^+$ and the average number of the Na-coordinated O$_w$ and O atoms as a function of c_{TT}. (e) Proportions of different solvation structures vs. c_{TT} (AGG: aggregates, CIP: contact ion pairs, SSIP: solvent-separated ion pairs, and free: free ions). (f) Diffusion coefficient of Na$^+$, D_{Na}, and viscosity of the electrolyte, η, as a function of c_{TT}.
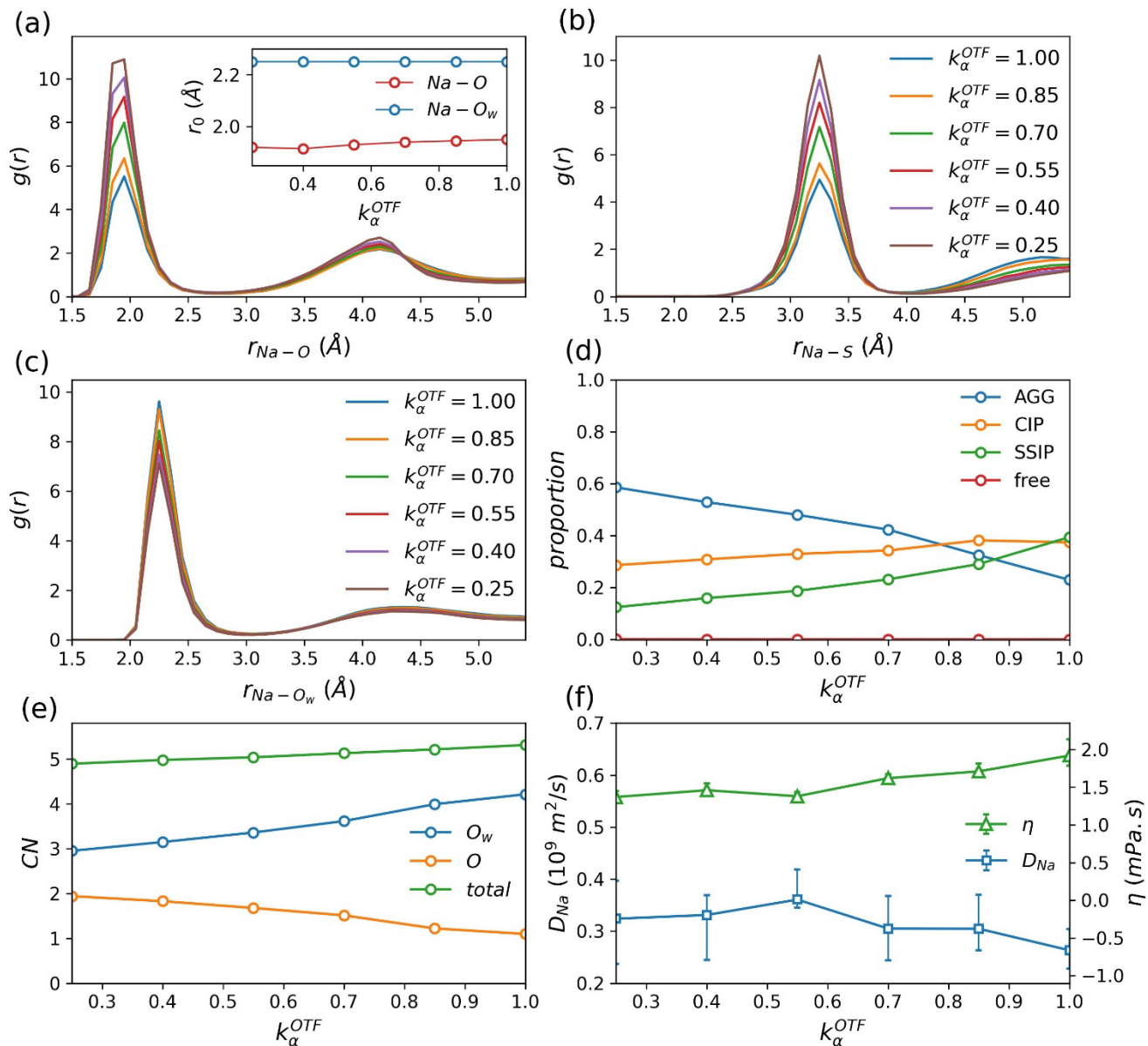
Figure 10. Dependence of the electrolyte properties on the scaling factor applied to the anion polarizability, $k_\alpha^{OTF} = \alpha^{i'}/\alpha^i$, with $\alpha^{i'}$ and α^i being the scaled and the original polarizabilities of the atoms of OTF⁻ anions, respectively (other force field parameters are set according to the base polarizable force field described in table 6): (a-c) Radial pair distribution functions (RDFs) of the Na-O, Na-S, and Na-O$_w$ pairs. The inset shows the positions of the first peaks in the Na-O and Na-O$_w$ RDFs as a function of k_α^{OTF}. (d) Total coordination number (CN) of Na⁺ and the average number of the Na-coordinated O$_w$ and O atoms vs. k_α^{OTF}. (e) Proportions of different solvation structures as a function of k_α^{OTF} (AGG: aggregates, CIP: contact ion pairs, SSIP: solvent-separated ion pairs, and free: free ions). (f) Variation of the diffusion coefficient of Na⁺, D_{Na}, and the viscosity of the electrolyte, η, with k_α^{OTF}.

Figure 11. Variation of the electrolyte properties with the Thole damping parameter, a, which is used in Eq. 11 (other force field parameters are set according to the base polarizable force field described in table 6): (a-c) Radial pair distribution functions (RDFs) of the Na-O, Na-S, and Na-O_w pairs. The inset shows the positions of the first peaks in the Na-O and Na-O_w RDFs as a function of a. (d) Total coordination number (CN) of Na^+ and the average number of the Na-coordinated O_w and O atoms as a function of a. (e) Proportions of different solvation structures vs. a (AGG: aggregates, CIP: contact ion pairs, SSIP: solvent-separated ion pairs, and free: free ions). (f) Variation of the diffusion coefficient of Na^+, D_{Na}, and the viscosity of the electrolyte, η, with a.

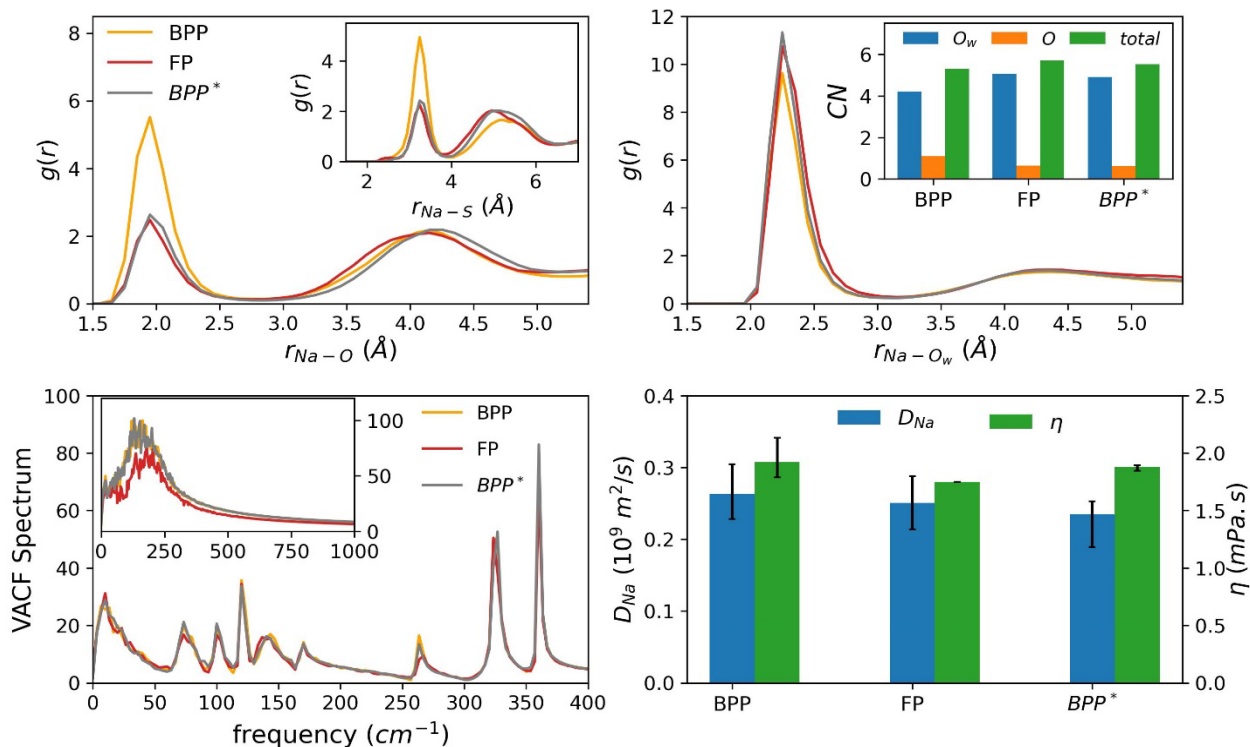### 3.4 Fully Polarizable force field

Finally, we set up a fully polarizable (FP) force field using SWM4-NDP method that explicitly model water polarization via Drude oscillators (see section 2.2.1). SWM4-NDP water parameters are listed in table 2 and other force field parameters are taken from the base partially polarizable (BPP) force field (see table 6). Fig. 12 shows that the BPP and FP force fields yield almost the same diffusion coefficients, viscosities, vibrational frequencies, and Na-OTF coordination modes, but they give different values for the number of Na-coordinated anions. We note that this difference can be reduced by adjusting the BPP force field parameters. For example, by using the Tang-Toennies damping parameter $b_{TT} = 4.59$, the BPP force field can reproduce the results of the FP simulation (see the results from the BPP* force field in Fig. 12). Since the SWM4-NDP model slows down the simulation due to the increased number of particles and bonds, and additionally exacerbates simulation stability issues, as discussed below, we suggest to use Drude polarizable force fields with non-polarizable water models, such as SPC/E, in future studies.

Figure 12. Electrolyte properties obtained using different polarizable force fields: the base partially polarizable (BPP) force field described in table 6, the fully polarizable (FP) force field, which is the same

as the BPP force field except that SPC/E water molecules are replaced with SWM4-NDP molecules, and the BPP* forcefield, which is identical to the BPP force field except that b_{TT} is set to 4.59. (a, b) Radial pair distribution functions (RDFs) of the Na-O, Na-S, and Na-O$_w$ pairs. The inset of panel (b) shows the total coordination number (CN) of Na$^+$ and the average number of the Na-coordinated O$_w$ and O atoms. (c) Vibrational spectra of ions (main panel) and water (inset). (d) Diffusion coefficient of Na$^+$, D_{Na}, and viscosity of the electrolyte, η, obtained using the studied force fields.

3.5 Simulation stability and runtime

As mentioned earlier, maintaining simulation stability is an important challenge when a Drude polarizable force field is used. In such a case, in addition to applying appropriate damping functions to short-distance electrostatic interactions (see Sec. 2.1.2, B), one must use a a sufficiently small time step to keep the simulation stable. For example, time steps larger than 0.5 fs in the BPP simulation (described in table 6) and time steps larger than 0.4 fs in the FP simulation (in the presence of SWM4-NDP water) cause instability, while the non-polarizable simulations remain stable with a large time step of $dt = 2\ fs$. A larger DP-DC force constant k_D can improve the stability of a Drude polarizable simulation, allowing for a larger time step. For example, in the stable BPP simulation with $k_D = 2000\ kcal/mol\ Å^2$, the time step is 3.33 times larger than the time step required at k_D=1000 $kcal/mol\ Å^2$ and 1.4 times smaller than the time step required at k_D=4000 $kcal/mol\ Å^2$. For k_D smaller than 1000 $kcal/mol\ Å^2$, the simulation persists unstable even though the time step is as small as 10^{-2} fs. Furthermore, a small k_D narrows the applicable range of the other Drude parameters (i.e., α^{Na}, α^{OTF}, k_D, b_{TT}, and c_{TT}) for stable simulations. It is, therefore, advantageous to set k_D to large enough values.

A major problem reported for Drude polarizable simulations is the flying ice cube artifact, which manifests itself in the faster-than-linear growth of the mean squared displacement with time, as explained in section 2.1.2, B. According to our investigations, this problem occurs when using the fully polarizable force field, regardless of the value of the force field parameters. In the case of partially polarizable force

fields, however, we encounter the problem only with $k_D = 1000 \, kcal/mol \, Å^2$, which is the smallest k_D we can use for a stable simulation. When the linear momentum is zeroed by subtracting the center-of-mass velocity from the atomic velocities every time step, the flying ice cube artifact can be avoided and the MSD vs t curve becomes perfectly linear. The inset of Fig. 13 shows the MSD from the simulation described in table 8 (4th row), before (BPP') and after (BPP'') zeroing the linear momentum.

In addition to the accuracy of the force field and the stability of the simulation, the computational cost is also an important factor for the appropriate choice of a force field. Fig. 13 shows the runtimes for force field simulations with considering different levels of dynamic polarization, as described in table 8. All these simulations are run for 24 ns on the bwForCluster JUSTUS2 HPC cluster using 48 CPU cores. The time step is set to 2 fs for the non-polarizable simulations BNP and BNP' while shorter time steps of 0.5 fs, 0.15 fs, and 0.4 fs are, respectively, used for the BPP, BPP', and FP simulations. In Fig. 13, the BNP simulation requires the lowest computational cost. The BNP' simulation is a bit slower due to the additional mass-less fourth site in the TIP4P water model. The reduced time step and the increased number of particles and bonds has significantly increased the runtime of the BPP simulation compared to the BNP and BNP' simulations. The BPP' simulation gets even slower than the BPP because of its very small time step. In the case of the FP simulation, Drude particles are also attached to water molecules, which increases the number of the particles and bonds compared to the BPP simulation and, consequently, makes the simulation much slower than the BPP simulation. It is worth noting that if one uses $k_D = k_D^{Ow} = 1000 \, kcal/mol \, Å^2$ in the fully polarizable simulation, the time step must be as small as 0.01 fs to make the simulation stable. Using this setup, the simulation will take about 250 days.
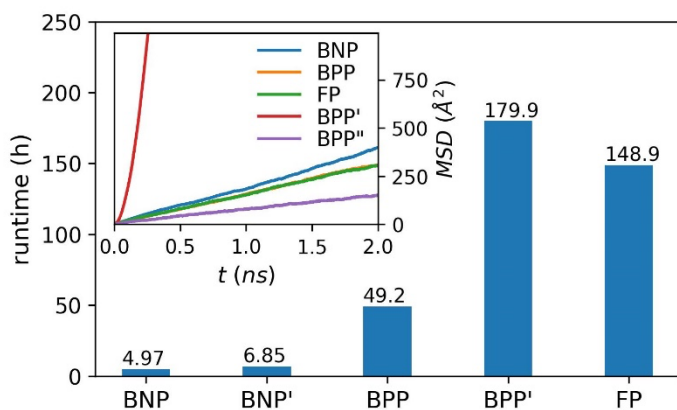
Figure 13. Runtimes for the simulations described in table 8 (main panel) and the resulting plot of mean-squared-displacement vs. time (inset). The red line in the inset shows the results obtained from the BPP' force field with the flying ice cube problem, and the purple line shows the results from the same force field when this problem is avoided by zeroing the linear momentum every time step.

Table 8. Force field and simulation parameter sets for performance testing

BNP	Base non-polarizable force field (parameters are given in table 6)
BNP'	The same parameters as in the BNP except that SPC/E water molecules are replaced with TIP4P molecules
BPP	Base partially polarizable force field (parameters are given in table 6)
BPP'	The same parameters as in the BPP simulation except that k_D is set to $1000\ kcal/mol\ Å^2$
FP	Fully polarizable force field (the same parameters as in the BPP force field except that SPC/E water molecules are replaced with SWM4-NDP molecules)

3.6 WiS electrolytes in rechargeable batteries

The results presented in this paper not only help in choosing an appropriate force field for molecular modeling of WiS electrolytes and in designing a proper protocol for force field parameterization, but they also provide a general insight into how WiS electrolytes work in rechargeable batteries. Most interestingly, our results indicate that a WiS electrolyte performs best in a battery when the proportion of CIPs is as high as possible, leading to the maximum possible ion diffusivity in the solution (see Figs. 6-9). As a result, the degree of salt dissociation and thus the solvation energy of ions should be optimized in order to reach the maximum efficiency of the battery: weak ion solvation reduces battery performance

through the formation of aggregates while excessive ion solvation is also undesirable not only because it slows down ion diffusion in the electrolyte, but also because it prevents ion desolvation at the electrodes and disrupts the intercalation process. Also, our results indicate that depending on the values set for the force field parameters (and assuming that the fully aggregated ionic structure never occurs in reality), the diffusion coefficient of Na$^+$ in the studied WiS solution is in the range of $10^{-10} - 10^{-9}\ m^2/s$, which is comparable to the values reported for Na$^+$ in organic electrolytes conventionally used in rechargeable batteries [26, 95-97]. Experimental measurements [98-100] and numerical calculations [101-105] indicate that the diffusion coefficient of Li$^+$ is in almost the same range (sometimes even lower) in different battery electrolytes. This means that with WiS electrolytes, water can be used in batteries as a safe, available, and environmentally friendly solvent, while the diffusion coefficient of ions, which is expected to be greatly reduced due to the very high salt concentrations of WiS solutions [26], is still within the working range of batteries.

Conclusion

A NaOTF Water-in-Salt (WiS) electrolyte is modeled using classical Molecular Dynamics (MD) simulations with four levels accounting for atomic polarization, which is of utmost importance in the molecular simulation of highly concentrated electrolytes. We consider first a non-polarizable all-atom force field with Lennard-Jones (LJ) and Coulomb potential interactions where an effective polarization is implicitly accounted for in the LJ interaction parameters. Second, on top of the non-polarizable force field, uniformly scaled ionic charges are considered, which supposedly account for average polarizability. Third, a partially polarizable force field is considered to explicitly model the atomic polarizability for salt ions via Drude oscillators while using the non-polarizable SPC/E water model. Finally, we consider a fully polarizable force field using Drude oscillators for both salt ions and water molecules. The electrolyte properties and their dependence on the force field parameters are probed by varying the parameters within a range where the simulation remains stable.

Our results indicate that the LJ parameters for the cations (here, Na$^+$) have a significant impact on both the solution structure and the dynamic properties of the electrolyte. These parameters not only adjust the size of the cations and the strength of their short-distance VdW interactions, but also have a major impact on the cation-anion coordination mode, and subsequently, on the solution structure. We also show that the well-known water models SPC, SPC/E, SPC/Fw, OPC3, TIP3P, and TIP4P provide almost the same properties for the studied WiS solution and thus the quality of the electrolyte simulations has no significant dependence on the water models. Uniform scaling of the ionic charges influences the electrolyte viscosity and the diffusion coefficient of cations. Such charge scaling, however, does not significantly affect the solution structure, except that it makes the first solvation shell around cations slightly more disordered. As a result, we suggest scaling down the ionic charges only to adjust the diffusion coefficient of cations while preserving the solvation structure in non-polarizable force field simulations.

When Drude oscillators model the dynamic polarization, the reduced time step and the damped short-distance dipolar interactions to make the simulation stable. In addition, when Drude particles are weakly bound to their core atoms or when water is modeled using the polarizable SWM4-NDP model, the linear momentum should be zeroed every time step to avoid the flying ice cube problem, which is an artifact that causes the mean square displacement to grow faster than linearly over time. The introduction of Drude oscillators extends the number of force field parameters for adjusting the electrolyte. Our results indicate that the Thole damping parameter a, which adjusts the short-distance dipole-dipole interactions, has only a minor effect on the properties of the studied WiS solution. The electrolyte properties are, however, significantly dependent on the other Drude parameters. The variation of Drude parameters changes the dissociation degree of NaOTF, which manifests itself in changed proportions of solvent-separated ion pairs (SSIPs) and aggregates (AGGs), and influences the number of cation-coordinated anions. The proportion of contact ion pairs (CIPs) first increases and then decreases with an increase in the salt dissociation degree, showing that some aggregates first break down into CIPs and then dissociate

into SSIPs. Dynamic properties of the electrolyte and the degree of salt dissociation are complicatedly related. Dissociation of ions decreases the number of aggregates, which tends to increase ion diffusivity due to the reduced size of the diffusing species, and increases the viscosity due to the reduced number of uncoordinated water molecules, which tends to reduce ion diffusivity. When the salt ions are either fully associated or fully dissociated, ion diffusivity is almost independent of the studied Drude parameters. When the salt ions are partly dissociated, the simultaneous action of the above factors causes non-monotonic variations in ion diffusion coefficient with Drude parameters. For the studied WiS electrolyte, the maximum Na^+ diffusivity occurs when SSIPs and AGGs have almost equal proportions while the proportion of CIPs is at its maximum.

Finally, the partially polarizable force field (combining the Drude polarizable force field and a non-polarizable water model) can reproduce the results obtained from the fully polarizable force field (polarizable simulations using the SWM4-NDP water model) by adjusting the Drude parameters. The SWM4-NDP water model requires an increased number of particles and bonds, thus causing a higher computational effort, and leads to stability problems because of the separate thermostat applied to the rigid SWM4-NDP water molecules. Therefore, we strongly recommend combining Drude polarizable force fields with non-polarizable water models, such as SPC/E, in the molecular modeling of WiS electrolytes.

ACKNOWLEDGMENTS

References

1.   Choi, S.; Wang, G., Advanced Lithium-Ion Batteries for Practical Applications: Technology, Development, and Future Perspectives. *Advanced Materials Technologies* **2018,** *3* (9), 1700376.

2.   Janek, J.; Zeier, W. G., A solid future for battery development. *Nature Energy* **2016,** *1* (9), 16141.

3.   Kalhoff, J.; Eshetu, G. G.; Bresser, D.; Passerini, S., Safer Electrolytes for Lithium-Ion Batteries: State of the Art and Perspectives. *ChemSusChem* **2015,** *8* (13), 2154-2175.

4.   Elia, G. A.; Marquardt, K.; Hoeppner, K.; Fantini, S.; Lin, R.; Knipping, E.; Peters, W.; Drillet, J.-F.; Passerini, S.; Hahn, R., An Overview and Future Perspectives of Aluminum Batteries. *Advanced Materials* **2016,** *28* (35), 7564-7579.

5.   Jäckle, M.; Helmbrecht, K.; Smits, M.; Stottmeister, D.; Groß, A., Self-diffusion barriers: possible descriptors for dendrite growth in batteries? *Energy & Environmental Science* **2018,** *11* (12), 3400-3407.

6.   Armand, M.; Endres, F.; MacFarlane, D. R.; Ohno, H.; Scrosati, B., Ionic-liquid materials for the electrochemical challenges of the future. *Nature Materials* **2009,** *8* (8), 621-629.

7.   Buchner, F.; Forster-Tonigold, K.; Bozorgchenani, M.; Gross, A.; Behm, R. J., Interaction of a Self-Assembled Ionic Liquid Layer with Graphite(0001): A Combined Experimental and Theoretical Study. *The Journal of Physical Chemistry Letters* **2016,** *7* (2), 226-233.

8.   Kim, H.; Hong, J.; Park, K.-Y.; Kim, H.; Kim, S.-W.; Kang, K., Aqueous Rechargeable Li and Na Ion Batteries. *Chemical Reviews* **2014,** *114* (23), 11788-11827.

9.   Wang, Y.; Yi, J.; Xia, Y., Recent Progress in Aqueous Lithium-Ion Batteries. *Advanced Energy Materials* **2012,** *2* (7), 830-840.

10.   Suo, L.; Borodin, O.; Gao, T.; Olguin, M.; Ho, J.; Fan, X.; Luo, C.; Wang, C.; Xu, K., "Water-in-salt" electrolyte enables high-voltage aqueous lithium-ion chemistries. *Science* **2015,** *350* (6263), 938-943.

11.   Suo, L.; Borodin, O.; Sun, W.; Fan, X.; Yang, C.; Wang, F.; Gao, T.; Ma, Z.; Schroeder, M.; von Cresce, A.; Russell, S. M.; Armand, M.; Angell, A.; Xu, K.; Wang, C., Advanced High-Voltage Aqueous Lithium-Ion Battery Enabled by "Water-in-Bisalt" Electrolyte. *Angewandte Chemie International Edition* **2016,** *55* (25), 7136-7141.

12.   Wang, Y.; Meng, X.; Sun, J.; Liu, Y.; Hou, L., Recent Progress in "Water-in-Salt" Electrolytes Toward Non-lithium Based Rechargeable Batteries. *Frontiers in Chemistry* **2020,** *8*.

13.   Suo, L.; Borodin, O.; Wang, Y.; Rong, X.; Sun, W.; Fan, X.; Xu, S.; Schroeder, M. A.; Cresce, A. V.; Wang, F.; Yang, C.; Hu, Y.-S.; Xu, K.; Wang, C., "Water-in-Salt" Electrolyte Makes Aqueous Sodium-Ion Battery Safe, Green, and Long-Lasting. *Advanced Energy Materials* **2017,** *7* (21), 1701189.

14.   Fichtner, M., Recent Research and Progress in Batteries for Electric Vehicles. *Batteries & Supercaps* **2022,** *5* (2), e202100224.

15.   Abraham, K. M., How Comparable Are Sodium-Ion Batteries to Lithium-Ion Counterparts? *ACS Energy Letters* **2020,** *5* (11), 3544-3547.

16.   Didar, B. R.; Groß, A., Solvation structure and dynamics of Li and LiO2 and their transformation in non-aqueous organic electrolyte solvents from first-principles simulations. *Chinese Journal of Catalysis* **2022,** *43* (11), 2850-2857.

17.   Borodin, O.; Suo, L.; Olguin, M.; Cresce, A. v.; Vatamanu, J.; Wang, F.; Ren, X.; Dura, J. A.; Faraone, A.; Gobet, M.; Munoz, S.; Greenbaum, S.; Wang, C.; Xu, K., Structure and Transport of "Water-in-Salt" Electrolytes from Molecular Dynamics Simulations. *ECS Meeting Abstracts* **2017,** *MA2017-02* (46), 2014.

18.   Zhang, Y.; Lewis, N. H. C.; Mars, J.; Wan, G.; Weadock, N. J.; Takacs, C. J.; Lukatskaya, M. R.; Steinrück, H.-G.; Toney, M. F.; Tokmakoff, A.; Maginn, E. J., Water-in-Salt LiTFSI Aqueous Electrolytes. 1. Liquid Structure from Combined Molecular Dynamics Simulation and Experimental Studies. *The Journal of Physical Chemistry B* **2021,** *125* (17), 4501-4513.

19.   Zhang, Y.; Maginn, E. J., Water-In-Salt LiTFSI Aqueous Electrolytes (2): Transport Properties and Li+ Dynamics Based on Molecular Dynamics Simulations. *The Journal of Physical Chemistry B* **2021,** *125* (48), 13246-13254.

20.   Mendez-Morales, T.; Li, Z.; Salanne, M., Computational Screening of the Physical Properties of Water-in-Salt Electrolytes**. *Batteries & Supercaps* **2021,** *4* (4), 646-652.

21.   Lim, J.; Park, K.; Lee, H.; Kim, J.; Kwak, K.; Cho, M., Nanometric Water Channels in Water-in-Salt Lithium Ion Battery Electrolyte. *Journal of the American Chemical Society* **2018,** *140* (46), 15661-15667.

22.   Triolo, A.; Di Lisio, V.; Lo Celso, F.; Appetecchi, G. B.; Fazio, B.; Chater, P.; Martinelli, A.; Sciubba, F.; Russina, O., Liquid Structure of a Water-in-Salt Electrolyte with a Remarkably Asymmetric Anion. *The Journal of Physical Chemistry B* **2021,** *125* (45), 12500-12517.

23.   Tirado-Rives, J. W. M. D., J. Development and testing of the OPLS all-atom force field on conformational energetics and properties of organic liquids. *J. Am. Chem. Soc* **1996,** *118* (45), 11225-11236.

24.   Wang, J.; Wolf, R. M.; Caldwell, J. W.; Kollman, P. A.; Case, D. A., Development and testing of a general amber force field. *Journal of Computational Chemistry* **2004,** *25* (9), 1157-1174.

25.   Gupta, S.; Sappidi, P., Understanding the Molecular-Level Structure and Dynamics of Sodium Ions in Water in Ionic Liquid Electrolytes by Molecular Dynamics Simulations. *Journal of Chemical & Engineering Data* **2022**.

26.   Sakti, A. W.; Wahyudi, S. T.; Ahmad, F.; Darmawan, N.; Hardhienata, H.; Alatas, H., Effects of Salt Concentration on the Water and Ion Self-Diffusion Coefficients of a Model Aqueous Sodium-Ion Battery Electrolyte. *The Journal of Physical Chemistry B* **2022,** *126* (11), 2256-2264.

27.   C. da Silva, D. A.; Pinzón C, M. J.; Messias, A.; Fileti, E. E.; Pascon, A.; Franco, D. V.; Da Silva, L. M.; Zanin, H. G., Effect of conductivity, viscosity, and density of water-in-salt electrolytes on the electrochemical behavior of supercapacitors: molecular dynamics simulations and in situ characterization studies. *Materials Advances* **2022,** *3* (1), 611-623.

28.   Kartha, T. R.; Mallik, B. S., Ionic conductance and viscous drag in water-in-salt electrolytes for lithium and sodium ion batteries and supercapacitors. *Materials Today Communications* **2020,** *25*, 101588.

29.   Jiang, L.; Liu, L.; Yue, J.; Zhang, Q.; Zhou, A.; Borodin, O.; Suo, L.; Li, H.; Chen, L.; Xu, K.; Hu, Y.-S., High-Voltage Aqueous Na-Ion Battery Enabled by Inert-Cation-Assisted Water-in-Salt Electrolyte. *Advanced Materials* **2020,** *32* (2), 1904427.

30.   Borodin, O., Polarizable Force Field Development and Molecular Dynamics Simulations of Ionic Liquids. *The Journal of Physical Chemistry B* **2009,** *113* (33), 11463-11478.

31.   Goloviznina, K.; Gong, Z.; Padua, A. A. H., The CL&Pol polarizable force field for the simulation of ionic liquids and eutectic solvents. *WIREs Computational Molecular Science* **2022,** *12* (3), e1572.

32.   Drude, P., *The theory of optics*. Longmans, Green: 1922.

33.   Kubisiak, P.; Eilmes, A., Molecular Dynamics Simulations of Ionic Liquid Based Electrolytes for Na-Ion Batteries: Effects of Force Field. *The Journal of Physical Chemistry B* **2017,** *121* (42), 9957-9968.

34.   Leontyev, I.; Stuchebrukhov, A., Accounting for electronic polarization in non-polarizable force fields. *Physical Chemistry Chemical Physics* **2011,** *13* (7), 2613-2626.

35.   Cui, K.; Yethiraj, A.; Schmidt, J. R., Influence of Charge Scaling on the Solvation Properties of Ionic Liquid Solutions. *The Journal of Physical Chemistry B* **2019,** *123* (43), 9222-9229.

36.   Duboué-Dijon, E.; Javanainen, M.; Delcroix, P.; Jungwirth, P.; Martinez-Seara, H., A practical guide to biologically relevant molecular simulations with charge scaling for electronic polarization. *The Journal of Chemical Physics* **2020,** *153* (5), 050901.

37.	Lemkul, J. A.; Huang, J.; Roux, B.; MacKerell, A. D., Jr., An Empirical Polarizable Force Field Based on the Classical Drude Oscillator Model: Development History and Recent Applications. *Chemical Reviews* **2016**, *116* (9), 4983-5013.

38.	Waibel, C.; Gross, J., Polarizable Transferable Anisotropic United-Atom Force Field Based on the Mie Potential for Phase Equilibria: Ethers, n-Alkanes, and Nitrogen. *Journal of Chemical Theory and Computation* **2019**, *15* (4), 2561-2573.

39.	Geerke, D. P.; van Gunsteren, W. F., On the Calculation of Atomic Forces in Classical Simulation Using the Charge-on-Spring Method To Explicitly Treat Electronic Polarization. *Journal of Chemical Theory and Computation* **2007,** *3* (6), 2128-2137.

40.	van Maaren, P. J.; van der Spoel, D., Molecular Dynamics Simulations of Water with Novel Shell-Model Potentials. *The Journal of Physical Chemistry B* **2001,** *105* (13), 2618-2626.

41.	Rupakheti, C. R.; MacKerell, A. D., Jr.; Roux, B., Global Optimization of the Lennard-Jones Parameters for the Drude Polarizable Force Field. *Journal of Chemical Theory and Computation* **2021,** *17* (11), 7085-7095.

42.	Harder, E.; Anisimov, V. M.; Vorobyov, I. V.; Lopes, P. E. M.; Noskov, S. Y.; MacKerell, A. D.; Roux, B., Atomic Level Anisotropy in the Electrostatic Modeling of Lone Pairs for a Polarizable Force Field Based on the Classical Drude Oscillator. *Journal of Chemical Theory and Computation* **2006,** *2* (6), 1587-1597.

43.	Goloviznina, K.; Canongia Lopes, J. N.; Costa Gomes, M.; Pádua, A. A. H., Transferable, Polarizable Force Field for Ionic Liquids. *Journal of Chemical Theory and Computation* **2019,** *15* (11), 5858-5871.

44.	Groß, A.; Sakong, S., Ab Initio Simulations of Water/Metal Interfaces. *Chemical Reviews* **2022,** *122* (12), 10746-10776.

45.	Clough, S. A.; Beers, Y.; Klein, G. P.; Rothman, L. S., Dipole moment of water from Stark measurements of H2O, HDO, and D2O. *The Journal of Chemical Physics* **1973,** *59* (5), 2254-2259.

46.	Lamoureux, G.; Harder, E.; Vorobyov, I. V.; Roux, B.; MacKerell, A. D., A polarizable model of water for molecular dynamics simulations of biomolecules. *Chemical Physics Letters* **2006,** *418* (1), 245-249.

47.	Taylor, T.; Schmollngruber, M.; Schröder, C.; Steinhauser, O., The effect of Thole functions on the simulation of ionic liquids with point induced dipoles at various densities. *The Journal of Chemical Physics* **2013,** *138* (20), 204119.

48.	Thole, B. T., Molecular polarizabilities calculated with a modified dipole interaction. *Chemical Physics* **1981,** *59* (3), 341-350.

49.   Tang, K. T.; Toennies, J. P., An improved simple model for the van der Waals potential based on universal damping functions for the dispersion coefficients. *The Journal of Chemical Physics* **1984,** *80* (8), 3726-3741.

50.   Goloviznina, K.; Gong, Z.; Costa Gomes, M. F.; Pádua, A. A. H., Extension of the CL&Pol Polarizable Force Field to Electrolytes, Protic Ionic Liquids, and Deep Eutectic Solvents. *Journal of Chemical Theory and Computation* **2021,** *17* (3), 1606-1617.

51.   Harvey, S. C.; Tan, R. K. Z.; Cheatham Iii, T. E., The flying ice cube: Velocity rescaling in molecular dynamics leads to violation of energy equipartition. *Journal of Computational Chemistry* **1998,** *19* (7), 726-740.

52.   Chiu, S.-W.; Clark, M.; Subramaniam, S.; Jakobsson, E., Collective motion artifacts arising in long-duration molecular dynamics simulations. *Journal of Computational Chemistry* **2000,** *21* (2), 121-131.

53.   Braun, E.; Moosavi, S. M.; Smit, B., Anomalous Effects of Velocity Rescaling Algorithms: The Flying Ice Cube Effect Revisited. *Journal of Chemical Theory and Computation* **2018,** *14* (10), 5262-5272.

54.   Lamoureux, G.; Roux, B. t., Modeling induced polarization with classical Drude oscillators: Theory and molecular dynamics simulation algorithm. *The Journal of Chemical Physics* **2003,** *119* (6), 3025-3039.

55.   Whitfield, T. W.; Varma, S.; Harder, E.; Lamoureux, G.; Rempe, S. B.; Roux, B., Theoretical Study of Aqueous Solvation of K+ Comparing ab Initio, Polarizable, and Fixed-Charge Models. *Journal of Chemical Theory and Computation* **2007,** *3* (6), 2068-2082.

56.   Rowley, C. N.; Roux, B. t., The Solvation Structure of Na+ and K+ in Liquid Water Determined from High Level ab Initio Molecular Dynamics Simulations. *Journal of Chemical Theory and Computation* **2012,** *8* (10), 3526-3535.

57.   Berendsen, H. J. C.; Postma, J. P. M.; van Gunsteren, W. F.; Hermans, J., Interaction Models for Water in Relation to Protein Hydration. In *Intermolecular Forces: Proceedings of the Fourteenth Jerusalem Symposium on Quantum Chemistry and Biochemistry Held in Jerusalem, Israel, April 13–16, 1981*, Pullman, B., Ed. Springer Netherlands: Dordrecht, 1981; pp 331-342.

58.   Wu, Y.; Tepper, H. L.; Voth, G. A., Flexible simple point-charge water model with improved liquid-state properties. *The Journal of Chemical Physics* **2006,** *124* (2), 024503.

59.   Berendsen, H. J. C.; Grigera, J. R.; Straatsma, T. P., The missing term in effective pair potentials. *The Journal of Physical Chemistry* **1987,** *91* (24), 6269-6271.

60.   Jorgensen, W. L.; Chandrasekhar, J.; Madura, J. D.; Impey, R. W.; Klein, M. L., Comparison of simple potential functions for simulating liquid water. *The Journal of Chemical Physics* **1983,** *79* (2), 926-935.

61.   Izadi, S.; Onufriev, A. V., Accuracy limit of rigid 3-point water models. *The Journal of Chemical Physics* **2016,** *145* (7), 074501.

62.   Canongia Lopes, J. N.; Pádua, A. A. H., Molecular Force Field for Ionic Liquids Composed of Triflate or Bistriflylimide Anions. *The Journal of Physical Chemistry B* **2004,** *108* (43), 16893-16898.

63.   Heid, E.; Szabadi, A.; Schröder, C., Quantum mechanical determination of atomic polarizabilities of ionic liquids. *Physical Chemistry Chemical Physics* **2018,** *20* (16), 10992-10996.

64.   Chandrasekhar, J.; Spellmeyer, D. C.; Jorgensen, W. L., Energy component analysis for dilute aqueous solutions of lithium(1+), sodium(1+), fluoride(1-), and chloride(1-) ions. *Journal of the American Chemical Society* **1984,** *106* (4), 903-910.

65.   Joung, I. S.; Cheatham, T. E., III, Determination of Alkali and Halide Monovalent Ion Parameters for Use in Explicitly Solvated Biomolecular Simulations. *The Journal of Physical Chemistry B* **2008,** *112* (30), 9020-9041.

66.   Noy, A.; Soteras, I.; Javier Luque, F.; Orozco, M., The impact of monovalent ion force field model in nucleic acids simulations. *Physical Chemistry Chemical Physics* **2009,** *11* (45), 10596-10607.

67.   Loche, P.; Steinbrunner, P.; Friedowitz, S.; Netz, R. R.; Bonthuis, D. J., Transferable Ion Force Fields in Water from a Simultaneous Optimization of Ion Solvation and Ion–Ion Interaction. *The Journal of Physical Chemistry B* **2021,** *125* (30), 8581-8587.

68.   Beglov, D.; Roux, B., Finite representation of an infinite bulk system: Solvent boundary potential for computer simulations. *The Journal of Chemical Physics* **1994,** *100* (12), 9050-9063.

69.   Oostenbrink, C.; Villa, A.; Mark, A. E.; Van Gunsteren, W. F., A biomolecular force field based on the free enthalpy of hydration and solvation: The GROMOS force-field parameter sets 53A5 and 53A6. *Journal of Computational Chemistry* **2004,** *25* (13), 1656-1676.

70.   Àqvist, J., Ion-water interaction potentials derived from free energy perturbation simulations. *The Journal of Physical Chemistry* **1990,** *94* (21), 8021-8024.

71.   Jensen, K. P.; Jorgensen, W. L., Halide, Ammonium, and Alkali Metal Ion Parameters for Modeling Aqueous Solutions. *Journal of Chemical Theory and Computation* **2006,** *2* (6), 1499-1509.

72.   Heid, E.; Boresch, S.; Schröder, C., Polarizable molecular dynamics simulations of ionic liquids: Influence of temperature control. *The Journal of Chemical Physics* **2020,** *152* (9), 094105.

73.   Mahan, G. D., Modified Sternheimer equation for polarizability. *Physical Review A* **1980,** *22* (5), 1780-1785.

74.   Yu, H.; Whitfield, T. W.; Harder, E.; Lamoureux, G.; Vorobyov, I.; Anisimov, V. M.; MacKerell, A. D., Jr.; Roux, B., Simulating Monovalent and Divalent Ions in Aqueous Solution Using a Drude Polarizable Force Field. *Journal of Chemical Theory and Computation* **2010,** *6* (3), 774-786.

75.   Li, H.; Ngo, V.; Da Silva, M. C.; Salahub, D. R.; Callahan, K.; Roux, B.; Noskov, S. Y., Representation of Ion–Protein Interactions Using the Drude Polarizable Force-Field. *The Journal of Physical Chemistry B* **2015,** *119* (29), 9401-9416.

76.   Jiménez-Ángeles, F.; Harmon, K. J.; Nguyen, T. D.; Fenter, P.; Olvera de la Cruz, M., Nonreciprocal interactions induced by water in confinement. *Physical Review Research* **2020,** *2* (4), 043244.

77.   Dočkal, J.; Lísal, M.; Moučka, F., Molecular Force Field Development for Aqueous Electrolytes: 2. Polarizable Models Incorporating Crystalline Chemical Potential and Their Accurate Simulations of Halite, Hydrohalite, Aqueous Solutions of NaCl, and Solubility. *Journal of Chemical Theory and Computation* **2020,** *16* (6), 3677-3688.

78.   Grossfield, A.; Ren, P.; Ponder, J. W., Ion Solvation Thermodynamics from Simulation with a Polarizable Force Field. *Journal of the American Chemical Society* **2003,** *125* (50), 15671-15682.

79.   Molina, J. J.; Lectez, S.; Tazi, S.; Salanne, M.; Dufrêche, J.-F.; Roques, J.; Simoni, E.; Madden, P. A.; Turq, P., Ions in solutions: Determining their polarizabilities from first-principles. *The Journal of Chemical Physics* **2011,** *134* (1), 014511.

80.   Sangster, M. J. L.; Atwood, R. M., Interionic potentials for alkali halides. II. Completely crystal independent specification of Born-Mayer potentials. *Journal of Physics C: Solid State Physics* **1978,** *11* (8), 1541.

81.   Li, M.; Zhuang, B.; Lu, Y.; Wang, Z.-G.; An, L., Accurate Determination of Ion Polarizabilities in Aqueous Solutions. *The Journal of Physical Chemistry B* **2017,** *121* (26), 6416-6424.

82.   Noskov, S. Y.; Lamoureux, G.; Roux, B., Molecular Dynamics Study of Hydration in Ethanol−Water Mixtures Using a Polarizable Force Field. *The Journal of Physical Chemistry B* **2005,** *109* (14), 6705-6713.

83.   Polak, E.; Ribiere, G., Note sur la convergence de méthodes de directions conjuguées. *Revue française d'informatique et de recherche opérationnelle. Série rouge* **1969,** *3* (16), 35-43.

84.   Dequidt, A.; Devémy, J.; Pádua, A. A. H., Thermalized Drude Oscillators with the LAMMPS Molecular Dynamics Simulator. *Journal of Chemical Information and Modeling* **2016,** *56* (1), 260-268.

85.   HOCKNEY, R. W.; Eastwood, J. W., *Computer Simulation Using Particles*. Adam Hilger: 1988.

86.   Plimpton, S., Fast Parallel Algorithms for Short-Range Molecular Dynamics. *Journal of Computational Physics* **1995,** *117* (1), 1-19.

87.   Martyna, G. J.; Klein, M. L.; Tuckerman, M., Nosé–Hoover chains: The canonical ensemble via continuous dynamics. *The Journal of Chemical Physics* **1992,** *97* (4), 2635-2643.

88.   Kamberaj, H.; Low, R. J.; Neal, M. P., Time reversible and symplectic integrators for molecular dynamics simulations of rigid molecules. *The Journal of Chemical Physics* **2005,** *122* (22), 224114.

89.   Lee, S. H.; Rasaiah, J. C., MOLECULAR DYNAMICS SIMULATION OF IONIC MOBILITY. I: ALKALI METAL CATIONS IN WATER AT 25 C. *Journal of Chemical Physics* **1994,** *101*, 6964-6974.

90.   Zheng, Y.; Zaoui, A., How water and counterions diffuse into the hydrated montmorillonite. *Solid State Ionics* **2011,** *203*, 80-85.

91.   Stokes, R., The diffusion coefficients of eight uni-univalent electrolytes in aqueous solution at 25. *Journal of the American Chemical Society* **1950,** *72* (5), 2243-2247.

92.   Bernard, O.; Cartailler, T.; Turq, P.; Bium, L., Mutual diffusion coefficients in electrolyte solutions. *Journal of Molecular Liquids* **1997,** *73-74*, 403-411.

93.   Bankura, A.; Carnevale, V.; Klein, M. L., Hydration structure of Na+ and K+ from ab initio molecular dynamics based on modern density functional theory. *Molecular Physics* **2014,** *112* (9-10), 1448-1456.

94.   Seo, D. M.; Borodin, O.; Balogh, D.; O'Connell, M.; Ly, Q.; Han, S.-D.; Passerini, S.; Henderson, W. A., Electrolyte Solvation and Ionic Association III. Acetonitrile-Lithium Salt Mixtures–Transport Properties. *Journal of The Electrochemical Society* **2013,** *160* (8), A1061.

95.   Landesfeind, J.; Hosaka, T.; Graf, M.; Kubota, K.; Komaba, S.; Gasteiger, H. A., Comparison of Ionic Transport Properties of Non-Aqueous Lithium and Sodium Hexafluorophosphate Electrolytes. *Journal of The Electrochemical Society* **2021,** *168* (4), 040538.

96.   Morales, D.; Chagas, L. G.; Paterno, D.; Greenbaum, S.; Passerini, S.; Suarez, S., Transport studies of NaPF6 carbonate solvents-based sodium ion electrolytes. *Electrochimica Acta* **2021,** *377*, 138062.

97.   Pham, T. A.; Kweon, K. E.; Samanta, A.; Lordi, V.; Pask, J. E., Solvation and Dynamics of Sodium and Potassium in Ethylene Carbonate from ab Initio Molecular Dynamics Simulations. *The Journal of Physical Chemistry C* **2017,** *121* (40), 21913-21920.

98.   Hayamizu, K.; Aihara, Y.; Arai, S.; Martinez, C. G., Pulse-Gradient Spin-Echo 1H, 7Li, and 19F NMR Diffusion and Ionic Conductivity Measurements of 14 Organic Electrolytes Containing LiN(SO2CF3)2. *The Journal of Physical Chemistry B* **1999,** *103* (3), 519-524.

99.   Capiglia, C.; Saito, Y.; Kageyama, H.; Mustarelli, P.; Iwamoto, T.; Tabuchi, T.; Tukamoto, H., 7Li and 19F diffusion coefficients and thermal properties of non-aqueous electrolyte solutions for rechargeable lithium batteries. *Journal of Power Sources* **1999,** *81-82*, 859-862.

100.   Hayamizu, K., Temperature Dependence of Self-Diffusion Coefficients of Ions and Solvents in Ethylene Carbonate, Propylene Carbonate, and Diethyl Carbonate Single Solutions and Ethylene Carbonate + Diethyl Carbonate Binary Solutions of LiPF6 Studied by NMR. *Journal of Chemical & Engineering Data* **2012,** *57* (7), 2012-2017.

101.   Ong, M. T.; Verners, O.; Draeger, E. W.; van Duin, A. C. T.; Lordi, V.; Pask, J. E., Lithium Ion Solvation and Diffusion in Bulk Organic Electrolytes from First-Principles and Classical Reactive Molecular Dynamics. *The Journal of Physical Chemistry B* **2015,** *119* (4), 1535-1545.

102.   Karatrantos, A.; Ohba, T.; Cai, Q., Diffusion of ions and solvent in propylene carbonate solutions for lithium-ion battery applications. *Journal of Molecular Liquids* **2020**.

103.   Neuhaus, J.; Bellaire, D.; Kohns, M.; von Harbou, E.; Hasse, H., Self-Diffusion Coefficients in Solutions of Lithium Bis(fluorosulfonyl)imide with Dimethyl Carbonate and Ethylene Carbonate. *Chemie Ingenieur Technik* **2019,** *91* (11), 1633-1639.

104.   Borodin, O.; Smith, G. D., LiTFSI Structure and Transport in Ethylene Carbonate from Molecular Dynamics Simulations. *The Journal of Physical Chemistry B* **2006,** *110* (10), 4971-4977.

105.   Wróbel, P.; Kubisiak, P.; Eilmes, A., MeTFSI (Me = Li, Na) Solvation in Ethylene Carbonate and Fluorinated Ethylene Carbonate: A Molecular Dynamics Study. *The Journal of Physical Chemistry B* **2021,** *125* (4), 1248-1258.